

# A partition-of-unity dual-weighted residual approach for multi-objective goal functional error estimation applied to elliptic problems

Bernhard Endtmayer<sup>1</sup> and Thomas Wick<sup>2,3</sup>

<sup>1</sup> Institute of Computational Mathematics, JKU Linz, Altenberger Str. 69, 4040 Linz, Austria, Endtmayer.Bernhard@gmx.at

<sup>2</sup> Centre de Mathématiques Appliquées, École Polytechnique, 91128 Palaiseau, France, thomas.wick@polytechnique.edu

<sup>3</sup> RICAM Linz, Altenberger Str. 69, 4040 Linz, Austria

October 5, 2016

## Abstract

In this work, we design a posteriori error estimation and mesh adaptivity for multiple goal functionals. The method of choice is based on a variational dual-weighted residual method in which localization is achieved with a partition-of-unity. The key advantage is that we avoid evaluation of face integrals since the strong form of the equations is not required. For treating multiple goal functionals we employ the dual-dual (i.e., a discrete error problem) approach and suggest an alternative way for its computation. Our algorithmic developments are substantiated for elliptic problems in terms of four different numerical tests that cover various types of challenges, such as singularities, different boundary conditions as well as different types of goal functionals. Moreover, several computations with higher-order finite elements are performed.

**Keywords.** finite element method; mesh adaptivity; dual-weighted residual; partition-of-unity; multi-objective goal functionals

## 1 Introduction

In many physical applications the target is to compute a quantity of interest up to a certain accuracy rather than the entire solution. Moreover, fluid flow (Navier-Stokes) and aerodynamics flow simulations as well as multiphysics problems such as fluid-structure interaction, fracture problems, poroelastic problems, Maxwell equations, magnetohydrodynamics are of importance. Here, several physical phenomena interact and consequently the accurate evaluation of more than one goal functional might be of interest. However, before we can address such nonlinear coupled PDEs, we need a reliable framework that is tested and validated for a single PDE, different boundary conditions, and different types of goal functionals.

In this study, accurate functional evaluations are based on adaptive mesh refinement. The method of choice is based on dual-weighted residual (DWR) a posteriori error estimation [8, 9]. In addition to the primal problem, a dual problem needs to be solved that provides (local) sensitivity measures with respect to an error goal functional. In the early stages, further extensions of the DWR method have been accomplished in [24, 2, 1, 23, 22, 16, 11, 7]. Most of these studies have in common that we need the strong formulation [9] for the error localization. A weak form with patched meshes has been proposed in [11]. One advantage of a weak localization of the DWR technique lies in its application to multiphysics problems because the classical localization works with strong (second-order) operators that are costly to evaluate and additionally (often several) face integration terms need to be evaluated.

Recently, in [26], another weakly-based localization technique has been suggested. It is straightforward to employ and easy to implement. Here (similar to [11]), partial integration back to the strong operator is not necessary. Therefore, no face terms need to be evaluated. Rather, solution information about neighboring cells (which is very important in particular for low-order finite elements [13]) is gathered by employing a partition-of-unity (PU) leading to a nodal-based error indicator representation. To realize the PU, a lowest order finite element is sufficient. We notice that a PU for strongly localized DWR error estimation has been previously suggested in [21].

On the other hand, Hartmann and Houston [19] and Hartmann [18] considered multiple target functionals. However, literature on this topic is rare and there exists a few other studies [20, 14, 28] from which [28] is quite recent. One crucial difficulty is the computational cost not only for single goal functional evaluations with the DWR method; namely a (linear) dual problem needs to be solved, but which additionally must deliver ‘more’ information than the primal problem and for this reason is usually more expensive than a linear primal problem. Of course, for nonlinear problems, solving the dual problem does only correspond to one additional Newton solve. Thus, the cost of the dual problem becomes much less significant.

For multiple goal functionals, say  $N$ , a naive approach would mean to solve  $N$  dual problems, which makes the method not attractive at all. Therefore, the authors of [19, 18] considered a dual-dual problem (which is equivalent to saying a discrete error problem), which only requires two additional solutions and therefore significantly reduces the computational cost.

Based on this approach we suggest two modifications in this work. First, we apply the PU-DWR method to multiple target functionals. Second, we propose an idea how to decouple the two additional problems (associated with the dual-dual problem) such that they can be performed in principle in parallel. These algorithmic developments are complemented with a series of numerical examples using the finite element method in which different challenges are addressed. In particular several higher-order finite element computations are provided, which have not yet been shown for such problems in existing literature.

This paper is organized as follows: In Section 2 the model problem is presented as well as the basics of DWR mesh adaptivity. Then, in Section 3, the approach for treating multiple goal functionals is presented. Next in Section 4 various numerical examples are presented that cover different aspects of smooth solutions, singularities, L-shaped and slit domains. For residual-based error estimates and adaptivity in form of graded-mesh refinement for L-shaped domains (and domains with other corners) we refer to [4]. We also consider different

boundary conditions of homogeneous and nonhomogeneous Dirichlet type and homogeneous Neumann type. Moreover, different types of goal functionals are taken into account such as point values, line integration, and domain integrals. Finally in Section 5, we recapitulate our findings and provide a few ideas for future work.

## 2 The DWR method for goal functional evaluations

In this section, we first provide the problem statement and spatial discretization. Then, we briefly review the DWR method for single goal functionals and recapitulate the partition-of-unity approach for goal functional evaluations.

### 2.1 The model problem

By  $\Omega \subset \mathbb{R}^d$  with  $d = 2$  we denote a domain with polygonal or polyhedral domain. On  $\Omega$ , we denote by  $(\cdot, \cdot)$  the  $L^2$ -inner product and by  $\|\cdot\|$  the corresponding  $L^2$ -norm. By  $\langle \cdot, \cdot \rangle$  we denote as usual the pairing between  $H^{-1}$  and  $H_0^1$  functions [15]. By  $H^{r+1}(\Omega)$  we denote the space of Lebesgue functions with square integrable weak derivatives up to degree  $r+1$ . In particular, by  $V := H_0^1(\Omega)$  we denote the space of  $H^1(\Omega)$  functions with trace zero on the boundary  $\partial\Omega$ . The diffusion problem for given data  $f \in L^2(\Omega)$ ,  $g_D$  and  $g_N$  is defined as

$$-\nabla \cdot (\alpha \nabla u) = f \quad \text{in } \Omega, \quad (1)$$

$$u = g_D \quad \text{on } \Gamma_D, \quad (2)$$

$$\alpha \nabla u \cdot n = g_N \quad \text{on } \Gamma_N, \quad (3)$$

where  $\alpha \in \mathbb{R}$  is the diffusion coefficient,  $\Gamma_D \cap \Gamma_N = \emptyset$ ,  $\Gamma_D \cup \Gamma_N = \partial\Omega$  and  $n$  is the normal vector. The non-homogeneous Dirichlet boundary condition  $g_D$  is imposed on  $\partial\Omega$  in the trace sense of a  $H^1$  function. The corresponding weak problem on the continuous level reads:

**Formulation 2.1.** Find  $u \in \{g_D + V\}$ :

$$(a \nabla u, \nabla \varphi) = \langle f, \varphi \rangle \quad \forall \varphi \in V,$$

where

$$\langle f, \varphi \rangle := \int_{\Omega} f(x) \varphi(x) dx + \int_{\Gamma_N} g_N(x) \varphi(x) ds_x.$$

The unknown solution  $u \in V$  is approximated in a finite dimensional function space  $V_h$ , which is discussed in Section 2.2.

### 2.2 Spatial discretization

All formulations in this work are spatially discretized with a Galerkin finite element scheme, introducing  $H^1$  conforming discrete spaces  $V_h \subset V$  consisting of functions  $Q_r^c$  of degree  $r$ . Specifically, we use isoparametric tensor-product finite elements. The definition of the discrete space reads:

$$V_h := \{v_h \in [C(\Omega)]^d, v_h|_K \in [Q_r^c(K)]^d \quad \forall K \in \mathcal{T}_h, v_h|_{\partial\Omega} = 0\}$$

on quadrilateral elements  $K$  with hanging nodes [12]. The corresponding mesh is denoted by  $\mathbb{T}_h$ . The discretization parameter is labeled by  $h$ . For convenience of the reader, we often denote explicitly the degree  $r$  for the spaces  $V_h^{(r)}$  in order to avoid misunderstanding. The discretized version reads:

**Formulation 2.2.** Find  $u_h \in \{g_D + V_h\}$ :

$$a(u_h, \varphi_h) = \langle f, \varphi_h \rangle \quad \forall \varphi_h \in V_h,$$

where

$$a(u_h, \varphi_h) := (\alpha \nabla u_h, \nabla \varphi_h).$$

### 2.3 A brief review for single goal functionals

In the following we describe the DWR method for linear goal functionals and linear primal problems. The aim is to compute a certain quantity of interest  $J(u)$  with a desired accuracy at low computational cost. Possible examples are mean values, line integration or point values:

$$J(u) = \int_{\Omega} u \, dx, \quad J(u) = \int_{\Gamma} \partial_n u \, dx, \quad J(u) = u(x_0, y_0).$$

However, such a goal functional is computed with a numerical method leading to a discrete version  $J(u_h)$ . Thus the key question is whether we can bound the error  $J(u) - J(u_h)$ . To address this question, we assign a dual problem: Find  $z \in V$ :

$$a(\psi, z) = J(\psi) \quad \forall \psi \in V.$$

Specifically, the dual bilinear form is defined as

$$a(\psi, z) = (\alpha \nabla \psi, \nabla z).$$

The boundary conditions on  $\Gamma_D$  are build into  $V$  and are of homogeneous Dirichlet type.

Existence and uniqueness of this adjoint solution follows by standard arguments. The regularity of  $z \in V$  depends on the regularity of the functional  $J$ . For  $J \in H^{-1}(\Omega)$  it holds  $z \in H^1(\Omega)$ . Given a more regular functional like the  $L^2$ -error  $J(\varphi) = \|e_h\|^{-1}(e_h, \varphi)$  with  $J \in L^2(\Omega)^*$ , it holds  $z \in H^2(\Omega)$  on suitable domains (convex polygonal or smooth boundary with  $C^2$ -parameterization).

Inserting as special test function  $\psi := u - u_h$  yields:

$$a(u - u_h, z) = J(u - u_h),$$

and therefore we have now a representation for the error in the goal functional.

In order to derive an error estimator, we use Galerkin orthogonality and insert the test function  $\psi_h$ :

$$a(u - u_h, z - \psi_h) = J(u - u_h).$$

Since  $\psi_h$  is an arbitrary discrete test function, we can for example use a projection  $\psi_h := i_h z$ :

$$a(u - u_h, z - i_h z) = J(u - u_h). \tag{4}$$



Since  $z$  is an unknown itself, we cannot yet simply evaluate the error estimator because  $z$  is only known analytically in very special cases. Consequently in order to obtain a computable error representation,  $z$  is approximated through a discrete function  $z_h \in V_h$ , that is (as the primal problem itself) obtained from

$$a(\psi_h, z_h) = J(\psi_h) \quad \forall \psi_h \in V_h. \quad (5)$$

Then:

$$a(u - u_h, z_h - i_h z_h) = J(u - u_h). \quad (6)$$

The difficulty is that if we compute the dual problem with the same polynomial degree as the primal problem, then  $z_h - i_h z_h \equiv 0$ , and thus the whole error identity defined in (6) would vanish:

$$J(u - u_h) \equiv 0.$$

To overcome this point, either a global-higher order approximation (using a higher order finite element), a solution on a finer mesh, or local higher-order approximation using a patch-wise higher-order interpolation can be adopted [9, 7]. Clearly, the last possibility is the cheapest. In this work, however, for simplicity, we simply used a global-higher order finite element of degree  $r + 1$  (in case that the primal problem has been computed with degree  $r$ ).

We finally end up with the (primal) error estimator:

$$a(u - u_h, z_h^{(r+1)} - i_h z_h^{(r+1)}) \approx J(u - u_h).$$

Thus, the error in the functional  $J(u - u_h)$  can be expressed in terms of a residual, that is weighted by (the local) adjoint sensitivity information  $z - i_h z$ .

As quality measure we use the effectivity index  $I_{eff}$ :

$$I_{eff}(u_h, z_h) = \frac{a(u - u_h, z_h^{(r+1)} - i_h z_h^{(r+1)})}{J(u) - J(u_h)} \rightarrow 1 \quad (h \rightarrow 0). \quad (7)$$

For the localization of the error on each cell or each degree of freedom, we forward the reader to the next two sections.

## 2.4 The classical way

We briefly recapitulate the classical way and then explain a variational technique that uses a partition-of-unity (PU). Both techniques have in common that they start from

$$J(u - u_h) = a(u - u_h, z - i_h z).$$

In the classical way, the error identity (4) is treated with integration by parts on every mesh element  $K \in \mathcal{T}_h$ , which yields:

$$J(u - u_h) = \sum_{K \in \mathcal{T}_h} \langle f + \nabla \cdot (\alpha \nabla u_h), z - i_h z \rangle_K + \int_{\partial K} \alpha \partial_n u_h \cdot (z - i_h z) \, ds. \quad (8)$$

This primal error estimator needs to be evaluated in the dual space. Here, we proceed as follows:

- Prolongate the primal solution  $u_h$  into the dual space;
- Next, we compute the interpolation  $i_h z_h^{(r+1)} \in Q_r$  w.r.t. to the primal space;
- Then, we compute  $z_h^{(r+1)} - i_h z_h^{(r+1)}$  (here,  $i_h z_h^{(r+1)}$  is prolonged to  $Q_{r+1}$  in order to compute the difference);
- Evaluate the duality product  $\langle \cdot, \cdot \rangle$  and face terms.

Now we have all ingredients to evaluate the error estimator. Following the usual procedure for residual based error estimators [29], we combine each two boundary integrals over element edges to a normal jump and proceed with Cauchy Schwarz to get

$$|J(u) - J(u_h)| \leq \eta := \sum_{K \in \mathcal{T}_h} \rho_K \omega_K, \quad (9)$$

with

$$\rho_K := \|f + \nabla \cdot (\alpha \nabla u_h)\|_K + \frac{1}{2} h_K^{-\frac{1}{2}} \|[\alpha \partial_n u_h]\|_{\partial K} \quad (10)$$

$$\omega_K := \|z - i_h z\|_K + h_K^{\frac{1}{2}} \|z - i_h z\|_{\partial K}, \quad (11)$$

where by  $[\alpha \partial_n u_h]$  we denote the jump of the  $u_h$  derivative in normal direction. On the outer Dirichlet boundary  $\Gamma_D$ , we set  $[\alpha \partial_n u_h] = 0$  and on the Neumann part we evaluate  $\alpha \partial_n u_h = g_N$ . The residual part  $\rho_K$  only contains the discrete solution  $u_h$  and the problem data.

## 2.5 A variational error estimator with PU localization

In this section, we recapitulate an alternative way and use a localization approach based on the variational formulation [26]. This idea combines the simplicity of the approach proposed in [11] (as it is given in terms of variational residuals) with a very simple structure. Localization is based on introducing a partition of unity (PU)  $\{\psi_1, \dots, \psi_M\} =: V_{PU}$  with  $\dim(V_{PU}) = M$  and the property  $\sum \psi_i \equiv 1$  and insert these functions into the global error identity (4):

**Proposition 2.3.** For the finite element approximation of Formulation 2.1, we have the a posteriori error estimate:

$$|J(u) - J(u_h)| \leq \eta := \sum_{i=1}^M |\eta_i| \quad (12)$$

where

$$\eta_i = \left\{ -a(u - u_h, (z_h^{(r+1)} - i_h z_h^{(r+1)})\psi_i) \right\},$$

and more specifically for our diffusion problem:

$$\eta_i = \left\{ \langle f, (z_h^{(r+1)} - i_h z_h^{(r+1)})\psi_i \rangle - (\alpha \nabla u_h, \nabla (z_h^{(r+1)} - i_h z_h^{(r+1)})\psi_i) \right\}. \quad (13)$$

To set-up the PU, one can simply work with lowest-order finite elements, i.e., a bilinear function on quadrilaterals in two dimensions. Thus, as finite element space we can choose  $V_{PU} := V_h^{(1)}$ .

The previous error indicators  $\eta_i$  are node-wise contributions of the error. Mesh adaptivity can be carried out in two ways:

- in a node-wise fashion: if a node  $i$  is picked for refinement, all elements touching this node will be refined.
- alternatively, one could also first assemble element wise for each  $K \in \mathcal{T}_h$  indicators by summing up all indicators belonging to nodes of this element and then carry out adaptivity in the usual element-wise way.

On adaptive meshes with hanging nodes, the evaluation of the PU indicator is straightforward: First, the partition of unity is assembled in (13) employing the basis functions  $\psi_i \in V_{PU}$  for  $i = 1, \dots, M$ . In a second step, the contributions belonging to hanging nodes are condensed in the usual way by distribution to the neighboring indicators. This localization technique can be readily applied to general meshes in two and three dimensions. As it has been already demonstrated for the similar approach (for a single goal functional) from [11], for instance for variational inequalities in solid mechanics [27] or fluid-structure interaction [25], a major advantage of a weak localization is the easy application to nonlinear coupled PDE systems, where the evaluation of strong residuals can be cumbersome, such as for instance in fluid-structure interaction [25, 31]. Specifically, a first application of PU-DWR to nonlinear-coupled PDE problems has been recently undertaken in [30]. Finally, we want to comment that it is well-known that for dual-weighted residual goal-oriented adaptivity we have no theoretical justification for convergence and optimality of the adaptive algorithm, but only excellent practical observations.

### 3 PU-DWR for multiple goal functionals

In the previous section we recapitulated the DWR method for computing a single goal functional. Now we assume that there are  $N$  linear functionals where  $N \in \mathbb{N}$ . Let  $\mathbb{J}$  be defined as  $\mathbb{J} := \{J_0, \dots, J_{N-1}\}$ . We can use (12) for each  $J_i \in \mathbb{J}$  where  $i \in \{0, \dots, N-1\}$  to compute the node-wise contributions of the error. But to do so we have to solve  $N$  dual problems. Therefore we seek a method to avoid these computations. We follow the idea of combining the functionals in  $\mathbb{J}$  from [19, 18]. We create a linear combination of the goal functionals to one functional  $\tilde{J}_c$  where

$$\tilde{J}_c(\psi) := \sum_{i=0}^{N-1} w_i J_i(\psi) \quad \forall \psi \in V, \quad (14)$$

where  $w_i \in \mathbb{R}$ . We call  $\tilde{J}_c$  the combined functional. Now we have to find out how to choose  $w_i$ . One crucial aspect is the sign of  $w_i$ , because it may lead to error canceling. Furthermore we are interested in having similar relative errors in our functional evaluations. One idea is to choose  $w_i$  as

$$w_i := \frac{\text{sign}(J_i(u) - J_i(u_h))\omega_i}{|J(u_h)|}, \quad (15)$$

where  $\omega_i$  describes some self-chosen but positive weights. This choice leads to no error canceling and also the relative errors we obtain are similar (if the weights  $\omega_i$  are almost

equal). But unfortunately we do not know  $J_i(u)$ . Hence we have to find a way to get  $\text{sign}(J_i(u) - J_i(u_h))$ . To do so we consider the dual-dual problem [19, 18]:

**Formulation 3.1** (Dual-dual problem). Find the error function  $e$  such that

$$a(e, \psi) = \langle R_{u_h}, \psi \rangle \quad \forall \psi \in V, \quad (16)$$

where  $\langle R_{u_h}, \psi \rangle := \langle f, \psi \rangle - a(u_h, \psi)$ .

By solving this problem we obtain  $e$  where  $e = u - u_h$  and therefore we can compute  $J_i(u) - J_i(u_h)$ . The dual-dual problem provides information with respect to the error in the goal functionals  $J_i(u)$ , but it does not yield local error information that are required for mesh refinement. Thus the solution is to solve both the dual-dual problem and a dual problem leading to two additional problems. In summary, using this approach for multiple goal functionals, three problems need to be solved: primal, dual, dual-dual.

For treating the dual-dual problem we again have to solve a PDE discretized by finite elements. For this problem we have to use a discrete subspace  $V_h^{(r+1)} \subset V$  which fulfills  $V_h \subsetneq V_h^{(r+1)}$  because otherwise  $\langle R_{u_h}, \psi_h \rangle = 0$  for all  $\psi_h \in V_h$ , which we need to avoid. Moreover, we have to solve the primal problem to compute  $u_h$  and then compute  $e$  as solution of the dual-dual problem, so we have to solve two systems sequentially.

The dependence of the dual and dual-dual problem slightly limits the possibility to further reduce the computational cost. Therefore, we suggest the following alternative in case we approximate the solution in our discrete subspace  $V_h^{(r+1)}$ , ( $r \geq 1$ ):

**Proposition 3.2.** Let  $a : V \times V \rightarrow \mathbb{R}$  be a bilinear form,  $f \in V^*$ , where  $V^*$  is the dual space of  $V$ , fulfilling the assumptions of Lax-Milgram (e.g., [15, 17]) and let  $u_h, u_h^{(2)}, e_h^{(2)}$  be the solutions of the problems, respectively: Find  $u_h \in V_h, e_h^{(2)}, u_h^{(2)} \in V_h^{(2)}$  such that

$$a(u_h, \psi_h) = \langle f, \psi_h \rangle \quad \forall \psi_h \in V_h, \quad (17)$$

$$a(u_h^{(2)}, \psi_h^{(2)}) = \langle f, \psi_h^{(2)} \rangle \quad \forall \psi_h^{(2)} \in V_h^{(2)}, \quad (18)$$

and

$$a(e_h^{(2)}, \psi_h^{(2)}) = \langle R_{u_h}, \psi_h^{(2)} \rangle \quad \forall \psi_h^{(2)} \in V_h^{(2)}, \quad (19)$$

where,  $V_h \subset V$ ,  $V_h^{(2)} \subset V$  and  $\langle R_{u_h}, \psi_h^{(2)} \rangle$  is defined as in Formulation 3.1. Then there exists a projection  $P_{[V_h^{(2)}]} : V \rightarrow V_h^{(2)}$  such that

$$e_h^{(2)} = u_h^{(2)} - P_{[V_h^{(2)}]} u_h. \quad (20)$$

Specifically, if  $V_h \subseteq V_h^{(2)}$ , it holds

$$e_h^{(2)} = u_h^{(2)} - u_h. \quad (21)$$

*Proof.* Let  $u_h$  be the solution of (17), then there exists a unique  $f_{u_h} \in V^*$  such that

$$a(u_h, \psi) = \langle f_{u_h}, \psi \rangle \quad \forall \psi \in V. \quad (22)$$

If we want to approximate the solution of (22) on the finite element space  $V_h^{(2)}$  we obtain the approximation  $u_{u_h}$  of  $u_h$  which is given by the unique solution of the problem: Find  $u_{u_h}^{(2)} \in V_h^{(2)}$  such that

$$a(u_{u_h}, \psi_h^{(2)}) = \langle f_{u_h}, \psi_h^{(2)} \rangle \quad \forall \psi_h^{(2)} \in V_h^{(2)}.$$

It can be shown that the mapping  $u_h \mapsto u_{u_h}$  is a projection which will be denoted by  $P_{[V_h^{(2)}]}$ .

For this projection holds:

$$a(\underbrace{u_h - P_{[V_h^{(2)}]} u_h}_{u_{u_h}}, \psi_h^{(2)}) = \langle f_{u_h}, \psi_h^{(2)} \rangle - \langle f_{u_h}, \psi_h^{(2)} \rangle = 0 \quad \forall \psi_h^{(2)} \in V_h^{(2)}.$$

Now a simple calculation shows

$$\begin{aligned} a(e_h^{(2)}, \psi_h^{(2)}) &= \langle R_{u_h}, \psi_h^{(2)} \rangle = \langle f, \psi_h^{(2)} \rangle - a(u_h, \psi_h^{(2)}) \\ &= a(u_h^{(2)}, \psi_h^{(2)}) - a(P_{[V_h^{(2)}]} u_h, \psi_h^{(2)}) \\ &= a(u_h^{(2)} - P_{[V_h^{(2)}]} u_h, \psi_h^{(2)}) \quad \forall \psi_h^{(2)} \in V_h^{(2)}. \end{aligned}$$

With the Lax-Milgram lemma we know that there is a unique solution in  $V_h^{(2)}$  we can conclude that  $e_h^{(2)} = u_h^{(2)} - P_{[V_h^{(2)}]} u_h$  hence

$$a(e_h^{(2)}, \psi_h^{(2)}) = \langle R_{u_h}, \psi_h^{(2)} \rangle = a(u_h^{(2)} - P_{[V_h^{(2)}]} u_h, \psi_h^{(2)}) \quad \forall \psi_h^{(2)} \in V_h^{(2)}.$$

And this shows the first statement (20). If  $V_h \subseteq V_h^{(2)}$  holds then  $P_{[V_h^{(2)}]} u_h = u_h$  because  $u_h \in V_h^{(2)}$  and henceforth (21) has been shown.  $\square$

*Remark 3.1.* The assumptions of the Lax-Milgram lemma can be relaxed by any condition which guarantees only that  $a(u, \psi) = \langle f, \psi \rangle$  for all  $\psi \in V$ , (17), (18) and (19) have unique solutions for all  $f \in V^*$ .

*Remark 3.2.* Furthermore, we notice that our previous theory does hold not only for  $V_h^{(1)} \subset V_h^{(r+1)}$  but for general spaces which are not necessarily subspaces of  $V_h^{(r+1)}$ .

**Corollary 3.3.** From Proposition 3.2 we obtain that if we work on the spaces  $V_h$  and  $V_h^{(r+1)}$  the error can be simply computed as:

$$e_h^{(r+1)} = u_h^{(r+1)} - u_h.$$

In particular, the two subproblems for obtaining  $u_h^{(r+1)}$  and  $u_h$  can be computed in parallel without communication using the spaces  $V_h$  and  $V_h^{(r+1)}$ .

Furthermore to avoid problems with prolongation operators in programming we can compute immediately  $J_i(u_h)$  and just communicate this value. With the help of Proposition 3.2, the combined functional  $\tilde{J}_c$  is approximated by  $J_c$  with

$$J_c(\psi) := \sum_{i=0}^{N-1} J_i(\psi) \frac{\text{sign}(J_i(u_h^{(r+1)}) - J_i(u_h))\omega_i}{|J_i(u_h)|} \quad \forall \psi \in V, \quad (23)$$

for some self-chosen but positive weights  $\omega_i \in \mathbb{R}$ . Now we can use the PU approach for the functional  $J_c$  in a similar way as discussed in [26], which results in

**Proposition 3.4.** For the finite element approximation of Formulation 2.1, and considering  $N$  goal functionals we have the a posteriori error estimate:

$$|J_c(u) - J_c(u_h)| \leq \eta := \sum_{i=1}^M |\eta_i| \quad (24)$$

where

$$\eta_i = \left\{ \langle f, (z_h^{(r+1)} - i_h z_h^{(r+1)})\psi_i \rangle - (\alpha \nabla u_h, \nabla (z_h^{(r+1)} - i_h z_h^{(r+1)})\psi_i) \right\}. \quad (25)$$

Specifically, the dual problem is given by: Find  $z_h \in V_h^{r+1}$  such that

$$a(\psi_h, z_h) = J_c(\psi_h) \quad \forall \psi_h \in V_h^{r+1},$$

for which  $J_c$  has been constructed by (23).

*Remark 3.3.* An advantage of this approach is that we have to solve (as in [19, 18]) only 2 linear systems instead of  $N$  and furthermore we do not lose the possibility of parallelization.

*Remark 3.4.* If we use the same finite element space for the second primal problem and the dual problem then we just have to assemble one matrix instead of the two system matrices  $A_{\text{primal}}, A_{\text{dual}}$  since it holds  $A_{\text{dual}} = A_{\text{primal}}^T$ .

### 3.1 The adaptive algorithm

Let error tolerances  $TOL_i$  be given for each  $J_i \in \mathbb{J}$  and  $i \in \{0, \dots, N-1\}$  where  $N$  is the number of functionals of interest. Mesh adaptation is realized by extracting local error indicators from the a posteriori error estimate in Proposition 3.4. To this end, we can adapt the mesh using the following strategy:

1. **Solve two primal problems:** Compute the primal solutions  $u_h$  and  $u_h^{(r+1)}$  for two finite element spaces, respectively. This can be done completely in parallel.
2. **Construct combined functional:** Construct  $J_c$  as in (23)
3. **Solve dual problem:** Compute the dual solution  $z_h^{(r+1)}$  by solving the dual problem  $a(\psi_h, z_h) = J_c(\psi_h)$  on a larger FE-space than for  $u_h$ .
4. **Estimate:**

- Determine the indicator  $\eta_i$  at each node  $i$  by (25).
- Compute the sum of all indicators  $\eta := \sum_i \eta_i$ .
- Check, if the stopping criterion is satisfied:

$$|J_c(u) - J_c(u_h)| \leq \eta < TOL_c$$

where  $TOL_c := \inf_{i \in \{0, \dots, N-1\}} \left\{ \frac{\omega_i TOL_i}{|J_i(u_h)|} \right\}$ . If this criterion is satisfied, stop computation since  $J_c(u_h)$  has been computed with desired accuracy. Otherwise, proceed to the following step.

5. **Mark** all cells  $K_i$  that touch nodes that have values  $\eta_i$  above the average  $\frac{\alpha\eta}{N}$  (where  $N$  denotes the total number of cells of the mesh  $\mathbb{T}_h$  and  $\alpha \approx 1$ ).
6. **Refine** the mesh.
7. **Go back to 1.**

*Remark 3.5.* The reason for the special choice of  $TOL_c$  is to ensure that for all functionals  $J_i$  holds that  $|J_i(u) - J_i(u_h)| < TOL_i$ .

*Remark 3.6.* Despite that we formulated our algorithm for  $r$  and  $r + 1$ , we notice that we could also have worked with the same polynomial degree but locally using finer meshes to obtain the second space. This is very similar to the various options that we have to approximate the dual problem itself as described in Section 2.3.

## 4 Numerical tests

In this section, we consider several numerical tests to substantiate our algorithmic developments. More specifically, the algorithm was tested for the Poisson equation. Furthermore, we used always  $\omega_i = 1$  for the weights in  $J_c$  (as in (23)) and for simplicity  $\alpha = 1$  (as in section 2.1) for the diffusion coefficient. In more detail, we analyze our algorithm for the following examples:

- **Example 1a,b:** smooth and discontinuous right hand sides on an L-shaped domain.
- **Example 2a,b:** eigenvalue of the Laplacian as right hand side on the unit square. In Example 2a, we particularly focus on whether global refinement can deliver better results than local refinement for one functional. In Example 2b, we use again the L-shaped domain and we are especially interested if the sign, i.e.,  $\text{sign}(J_i(u_h^{(r+1)}) - J_i(u_h))$ , needs to be computed in every step.
- **Example 3:** singular right hand side  $f$  for which  $f \notin L^2(\Omega)$  but  $f \in L^{2-\varepsilon}(\Omega)$  for all  $\varepsilon > 0$  on an L-shaped domain. Here, we also perform comparisons with higher-order finite elements.
- **Example 4a,b:** zero right hand side on a slit domain with non-homogeneous Dirichlet and homogeneous Neumann conditions. In Example 4b, we focus again on higher-order computations.

For all examples in this section we always consider the error in  $J$  as the relative error  $\frac{|J(u_h) - J(u)|}{|J(u_h)|}$ . Furthermore we consider one refinement step for global refinement as refining every single element and one refinement step for DWR as one step of algorithm 3.1. The corresponding programming code is based on the open-source finite element package deal.II [6, 5].

## 4.1 Example 1

### 4.1.1 Example 1a

**Configuration** In the first example we considered the Poisson equation on an L-shaped domain  $\Omega = (-1, 1) \times (-1, 1) \setminus (-1, 0) \times (-1, 0)$  with smooth right hand side.

$$-\Delta u(x, y) = f(x, y) \quad \forall (x, y) \in \Omega, \quad (26)$$

$$u(x, y) = 0 \quad \forall (x, y) \in \partial\Omega, \quad (27)$$

where

$$f(x, y) = x(8 - 2x^2 - 6y^2 + e^{3y}(1 - 3y(4 + y) + x^2(-7 + 3y(4 + 3y))). \quad (28)$$

Here the exact solution  $u$  is given by

$$u(x, y) = x(y^2 - 1)(x^2 - 1)(e^{3y} - 1). \quad (29)$$

**Goal functionals of interest** We consider the following three goal functionals:

$$J_0(u) := u(0.5, 0.5), \quad J_1(u) := \int_{\Omega_1} u(x, y) d(x, y), \quad J_2(u) := \int_{\Gamma_1} \nabla u(x, y) \cdot n \, d(x, y),$$

where  $\Omega_1 = (-0.5, 0) \times (0.5, 1)$  and  $\Gamma_1 = \{1\} \times (0, 1)$ .

**Details on discretization** To solve the first primal problem (to obtain  $u_h$  as discussed in section 3) we used the Galerkin finite element scheme with the discrete space  $V_h \subset V$ . Here  $r = 1$ , which results in the space of bilinear functions  $Q_1^c$  on quadrilateral elements with hanging nodes. For hanging nodes we refer to [12]. For the second primal problem (to obtain  $u_h^{(2)}$  as discussed in section 3) and the dual problem we used the discrete space  $V_h^{(2)} \subset V$  which is the space of  $Q_2^c$  functions on the same quadrilateral elements as in  $V_h$ .

**Discussion of our findings** First of all we take a look at the  $I_{eff}$  (as in (7)) for  $J_c$  which measures how good we estimate the true error of  $J_c$  with our error estimator. In Figure 1 we observe that for this problem we obtain  $I_{eff} \approx 1$  which shows that we almost approximate the real error with our error estimator.



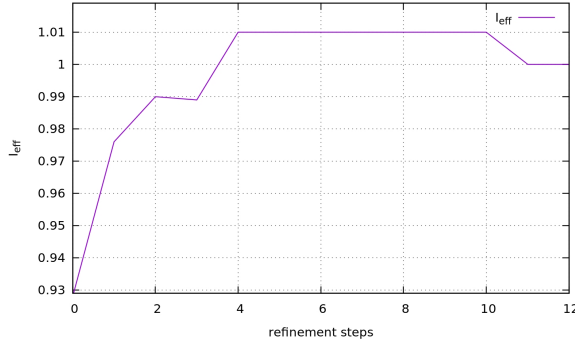


Figure 1: Example 1a:  $I_{eff}$  for  $J_c$  vs. refinement steps.

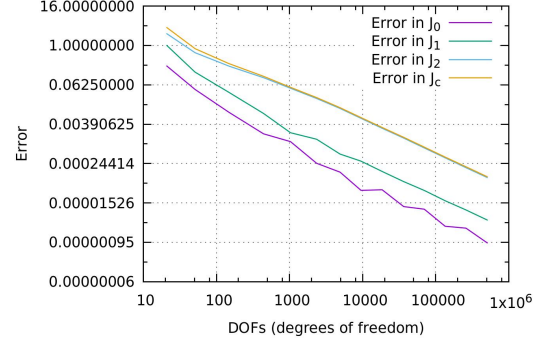


Figure 2: Example 1a: Comparison of relative errors.

In the following, let us have a look at the errors in the goal functionals  $J_i$ . In Figure 2 we observe that the error in  $J_c$  nearly approximates the functional with the largest error. Furthermore we recognize that the error in the other functionals behaves more inconsistent with more than 1000 DOFs. We compare the error using local mesh refinement with the error using global refinement for the single goal functionals.

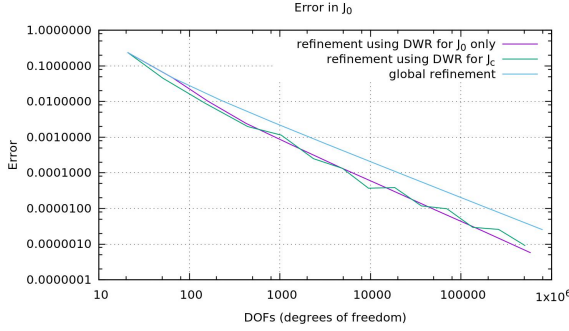


Figure 3: Example 1a: Comparison of relative errors for different refinements for  $J_0$ .

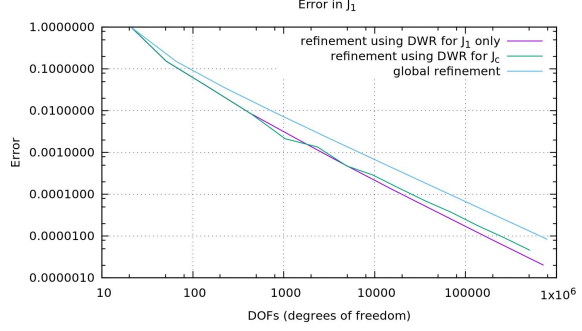


Figure 4: Example 1a: Comparison of relative errors for different refinements for  $J_1$ .

The relative error for the refinement for  $J_c$  shown in Figure 3 decreases almost as well as if we just use DWR for  $J_0$ . The relative error is less than  $10^{-5}$  with approximately  $7 \times 10^4$  DOFs (degrees of freedom) for DWR for  $J_c$ ,  $5 \times 10^4$  DOFs for DWR for  $J_0$  and  $25 \times 10^4$  DOFs for global refinement. Therefore both refinements deliver better results than global refinement. The same behavior also appears for the error in  $J_1$  shown in Figure 4. But the most interesting part is the error in  $J_2$  shown in Figure 5.

From the observation in Figure 2, we deduce that  $J_c$  shows similar behavior as the functional with the largest error. At the beginning of the algorithm we observe that we have worse convergence for refinement with respect to  $J_c$  than for the refinement versus  $J_2$ , but later we achieve a very similar rate because the weight  $w_2$  is the dominating one. For the error in  $J_2$  we obtain a big advantage. To get an error below  $10^{-2}$  we just need approximately 5000 DOFs instead of  $5 \times 10^4$  and to get an error below  $10^{-3}$  we need for global refinement more than  $10^6$  DOFs and we just need about  $5 \times 10^4$ , so we obtain an error

of  $10^{-3}$  instead of  $10^{-2}$  for the same number of DOFs. However, the results we obtained are not as good as when using DWR just for  $J_2$  through the effect at the beginning, but we also get the reduction in the other functionals of interest.

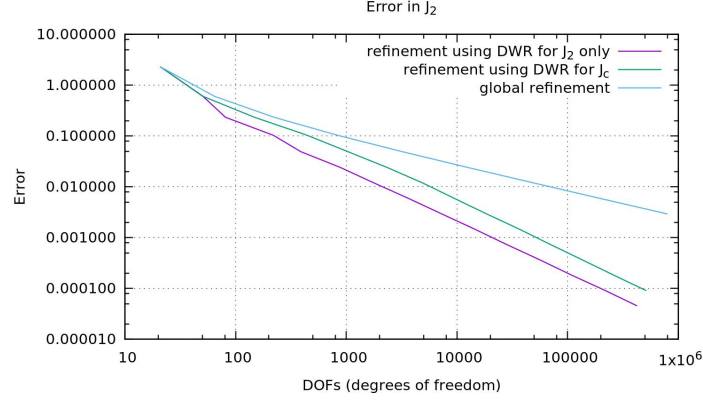


Figure 5: Example 1a: Comparison of relative errors for different refinements for  $J_2$ .

Finally we take a look at the refined meshes in Figures 6 - 9. The corresponding initial mesh is displayed in Figure 14. We observe that the mesh created by refinement with respect to  $J_c$  looks like a combination of the meshes where refinement for one functional is used. We monitor that  $J_2$  is again the dominating part in  $J_c$ .

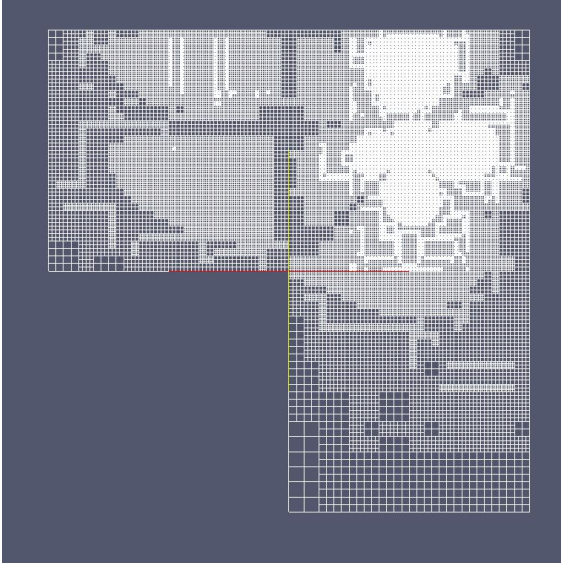


Figure 6: Example 1a: Mesh for DWR for  $J_0$  after 7 refinement steps.

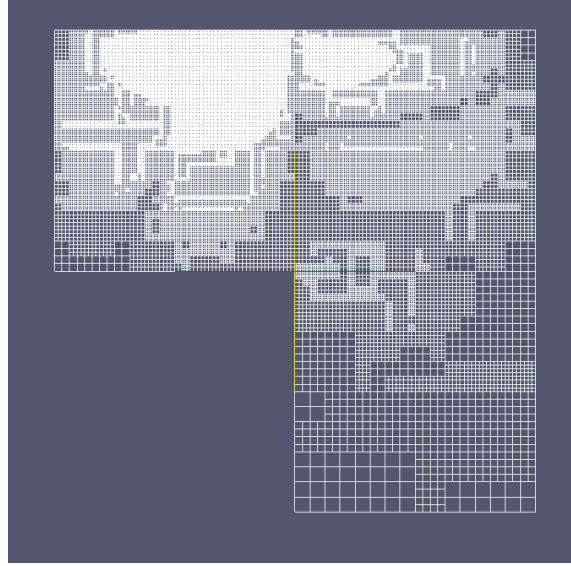


Figure 7: Example 1a: Mesh for DWR for  $J_1$  after 7 refinement steps.

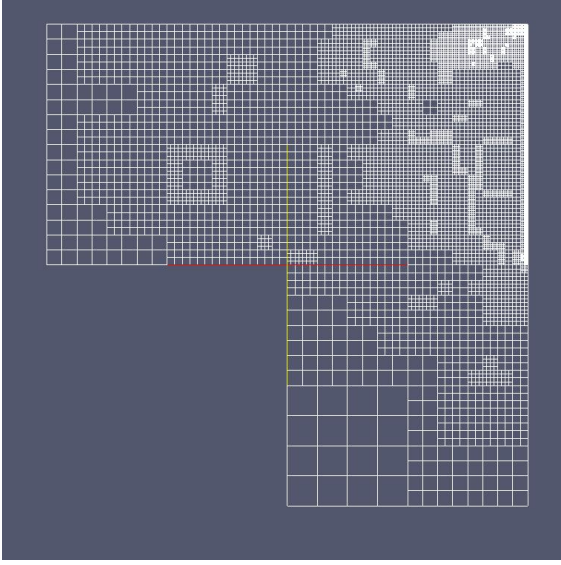


Figure 8: Example 1a: Mesh for DWR for  $J_2$  after 9 refinement steps.

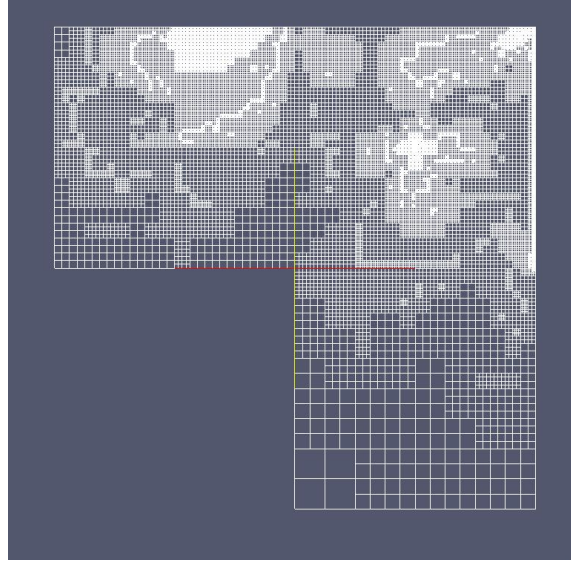


Figure 9: Example 1a: Mesh for DWR for  $J_c$  after 9 refinement steps.

#### 4.1.2 Example 1b

In this part, we work with the same domain and same discretization as before, but consider a discontinuous right hand side

$$f(x, y) = \begin{cases} \sqrt{|x|} + \sqrt{|y|} & \text{if } x^2 + y^2 < 1 \\ -x^2 + y & \text{else.} \end{cases}$$

Here no exact solution  $u$  is known.

**Goal functionals of interest** We consider the following three goal functionals:

$$J_0(u) := u(0.5, 0.5), \quad J_1(u) := \int_{\Omega_2} u(x, y) d(x, y), \quad J_2(u) := \int_{\Gamma_2} \nabla u(x, y) \cdot n \, d(x, y), \quad (30)$$

where  $\Omega_2 = (-1, -0.5) \times (0, 0.5)$  and  $\Gamma_2 = \{1\} \times (0, 1)$ . Since the exact solution is not known, we approximate the exact functional values by:

- $J_0(u) \approx 0.15389345606$ ,
- $J_1(u) \approx -0.012801283700$ ,
- $J_2(u) \approx -0.36864857768$ .

**Discretization** As in Example 1a.

**Discussion of our findings** The effectivity index  $I_{eff}$  in this case is shown in Figure 10. It is not as close to 1 as for Example 1a. This may happen through the loss of regularity.

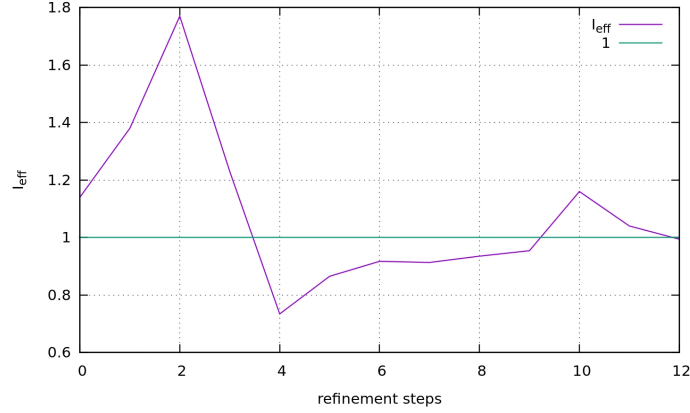


Figure 10: Example 1b:  $I_{eff}$  for  $J_c$  vs. refinement steps.

Hence we do not always get the optimal refinement. As before, the interesting part is the error in the functionals which is analyzed in Figure 11. We detect that the decrease of the error in  $J_c$  is again similar to the decrease of the functional with the largest error. Hence  $J_c$  changes the behavior after the error of  $J_2$  starts to dominate. As it can be seen in Figure 12, the refinement with respect to  $J_c$  even delivers worse results for  $J_0$  than for global refinement at the beginning, but we get a better decrease in the error afterwards. This raises the question whether it can happen that the refinement with respect to  $J_c$  does deliver a worse error than global refinement with the same number of DOFs for a single functional. This question will be answered in Example 2a. In  $J_2$  we again monitor a similar behavior as in Example 1a. To achieve an error less than  $10^{-3}$  we have to use approximately  $10^6$  DOFs and for the refinement with respect to  $J_c$  we just need approximately  $3 \times 10^4$  DOFs. However we see that the error in  $J_2$  even increases for one refinement step and this occurs in the global and the refinement for  $J_c$ .

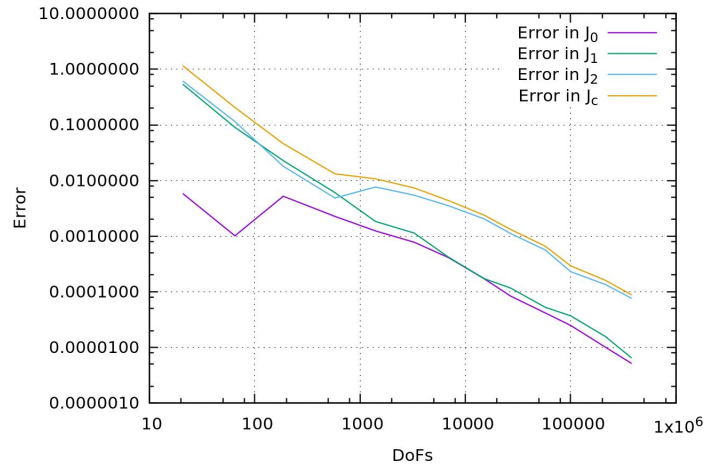


Figure 11: Comparison of relative errors.

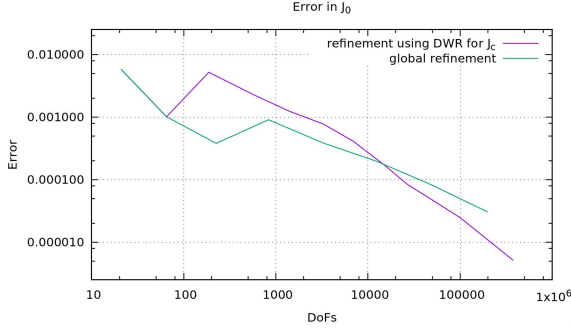


Figure 12: Example 1b: Comparison of relative errors for different refinements for  $J_0$ .

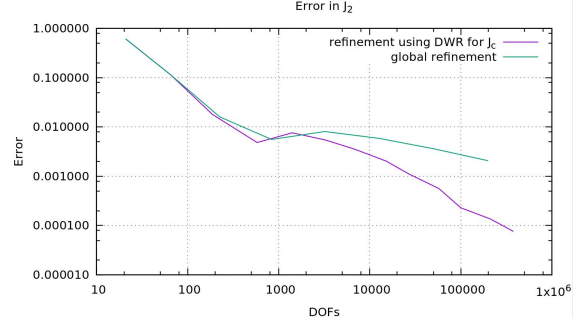


Figure 13: Example 1b: Comparison of relative errors for different refinements for  $J_2$ .

If we take a look at the mesh we can also see that the DWR method captures low regularity areas like the vertex  $(0,0)$  in the corner of the L-shaped domain.

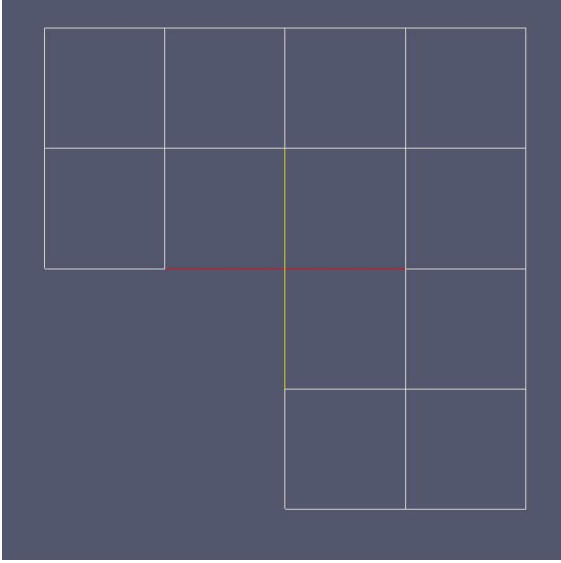


Figure 14: Initial mesh used in Example 1, 2a, and 3.

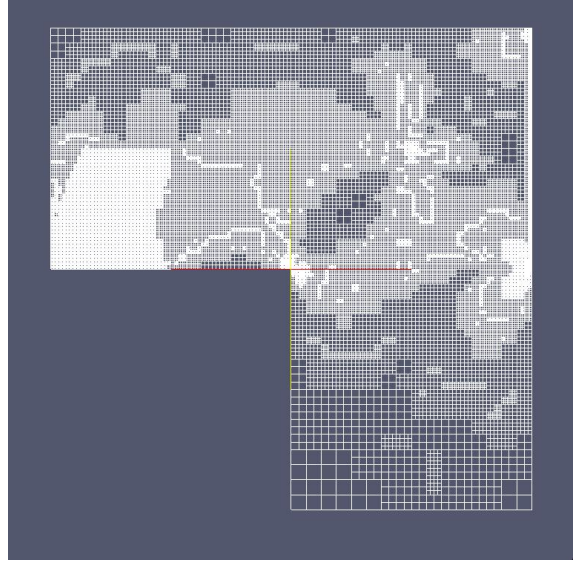


Figure 15: Example 1b: Mesh for DWR for  $J_c$  after 9 refinement steps.

## 4.2 Example 2

In this example we consider an eigenfunction of the Laplacian as right hand side on the unit square  $\Omega = (0,1) \times (0,1)$  and L-shaped domain  $\Omega = (-1,1) \times (-1,1) \setminus (-1,0) \times (-1,0)$ , respectively, with homogeneous Dirichlet boundary condition. The discretization is the same as in Section 4.1.

#### 4.2.1 Example 2a

**Configuration** Find  $u$  such that

$$-\Delta u(x, y) = f(x, y) \quad \forall (x, y) \in \Omega, \quad (31)$$

$$u(x, y) = 0 \quad \forall (x, y) \in \partial\Omega, \quad (32)$$

where

$$f(x, y) = 10 \sin(\pi x) \sin(3\pi y). \quad (33)$$

The exact solution  $u$  is given by

$$u(x, y) = \frac{\sin(\pi x) \sin(3\pi y)}{\pi^2}. \quad (34)$$

**Goal functionals of interest** We consider the following three goal functionals:

$$J_0(u) := u(0.5, 0.5), \quad J_1(u) := u(0.75, 0.25), \quad J_2(u) := \int_{\Gamma_3} \nabla u(x, y) \cdot n \, d(x, y), \quad (35)$$

where and  $\Gamma_3 = \{1\} \times (0, 1)$ .

**Discretization** As in Example 1a.

**Discussion of our findings** The effectivity index  $I_{eff}$  has values in  $(1.06, 1.45)$ , which is better than in Example 1b but worse than in Example 1a.

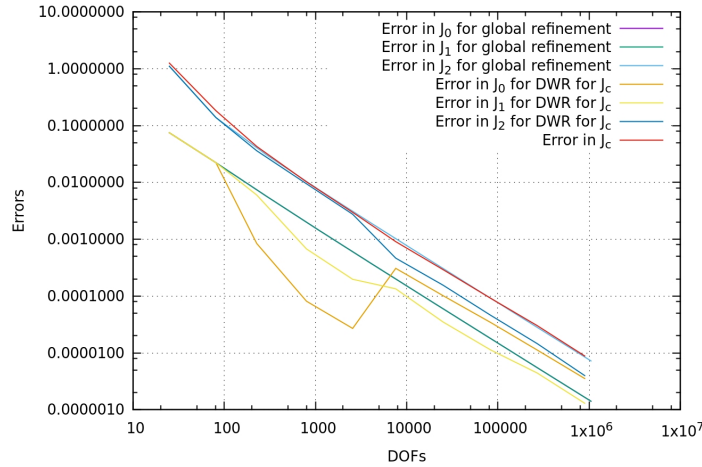


Figure 16: Comparison of relative errors for Example 2a. We note that the error in  $J_0$  and  $J_1$  for global refinement coincides.

With regard to the error, we make the following observations. In Figure 16 it is observed that we hardly achieve an advantage at the beginning for  $J_2$ , but at one specific refinement step we get a much better decrease in the error than in the other steps. But in this step we also get a worse error reduction in the other functionals and in  $J_0$  even an increase.



We also observe that we do not necessarily obtain a better result for one functional (here  $J_0$ ) if we use DWR with respect to  $J_c$  than for global refinement. An interesting fact is that the errors of  $J_0$  and  $J_1$  exactly coincide for global refinement but for the refinement using  $J_c$  they do not. One reason could be that the errors accumulate and therefore some of the refinement areas for the single functionals are geometrically connected (as visualized in Figure 18).

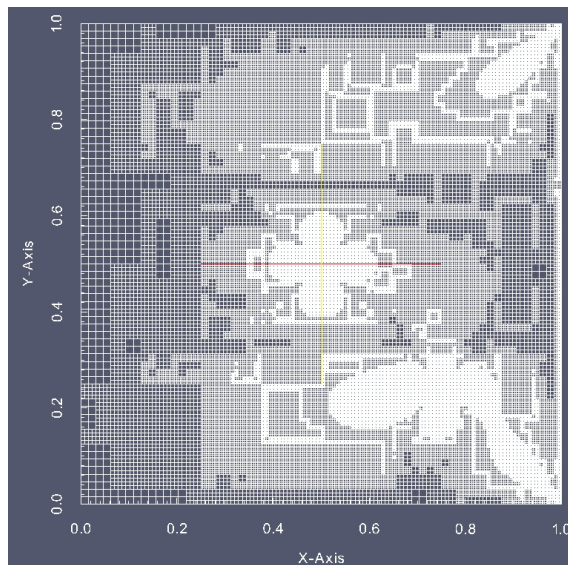
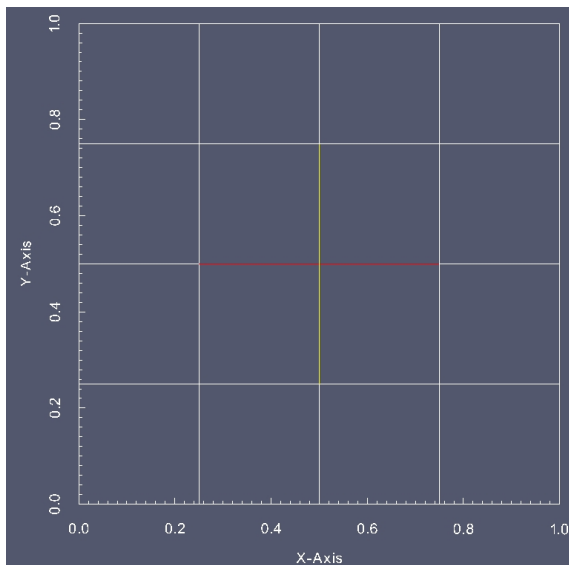


Figure 17: Initial mesh used for Example 2a. Figure 18: Mesh after 7 refinement steps for Example 2a.

#### 4.2.2 Example 2b

In the second part of Example 2, we compute now on an L-shaped domain with other functionals of interest and we investigate the sign of the combined functional  $J_c$ .

**Goal functionals of interest** We consider the following three goal functionals:

$$J_0(u) := u(0.5, 0.5), \quad J_1(u) := \int_{\Omega_4} u(x, y) d(x, y), \quad J_2(u) := \int_{\Gamma_4} \nabla u(x, y) \cdot n \, d(x, y), \quad (36)$$

where  $\Omega_4 = (0.75, 1) \times (0, 0.25)$  and  $\Gamma_4 = \{1\} \times (0, 1)$ .

**Discretization** As in Example 1a.

**Discussion of our findings** The relevant effectivity index  $I_{eff}$  is always in  $(1.03, 1.08)$  except on the coarsest mesh in step 0 where  $I_{eff} = 0.75$ . In the examples before we were mostly concerned about the error. But if we construct  $J_c$  as in (23) we have (as explained in section 3.1) to solve a bigger linear system just to get a sign for each weight. The question is whether this is really necessary. Therefore we investigate the dual solution in more detail.

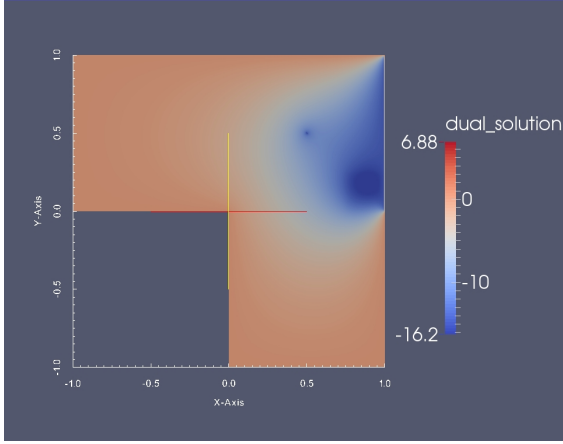


Figure 19: Example 2b: Dual solution after 6 refinement steps.

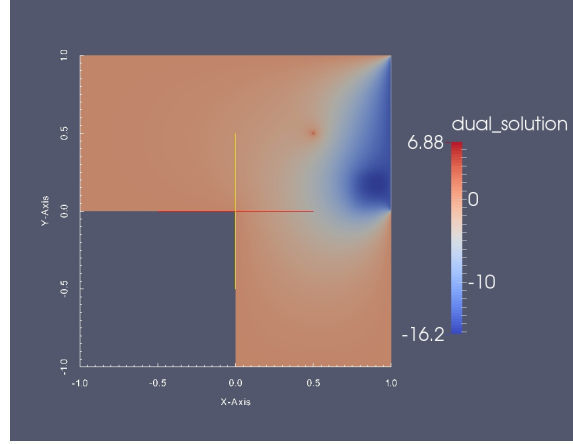


Figure 20: Example 2b: Dual solution after 7 refinement steps.

If we compare the Figures 19 and 20 we monitor there is indeed a change of the sign of  $w_0$  (as defined in (15)) during the computation. Hence the computation of the sign cannot be avoided in the Algorithm presented in Section 3.1.

### 4.3 Example 3

In this numerical test we consider a nonhomogeneous Dirichlet boundary condition on the L-shaped. The right hand side is non-homogeneous and has a pole at  $(0,0)$ . Moreover, we perform computations with higher-order finite elements.

**Configuration** Find  $u$  such that:

$$-\Delta u(x, y) = -\frac{1}{\|(x, y)\|_{l_2}} \quad \forall (x, y) \in \Omega, \quad (37)$$

$$u(x, y) = \|(x, y)\|_{l_2} \quad \forall (x, y) \in \partial\Omega, \quad (38)$$

where

$$\Omega = (-1, 1) \times (-1, 1) \setminus (-1, 0) \times (-1, 0). \quad (39)$$

The exact solution  $u$  is given by

$$u(x, y) = \|(x, y)\|_{l_2}. \quad (40)$$

**Goal functionals of interest** We consider the following three goal functionals:

$$J_0(u) := u(0.5, -0.5), \quad J_1(u) := u(0.5, 0.5), \quad J_2(u) := \int_{\Gamma_5} \nabla u(x, y) \cdot n \, d(x, y), \quad (41)$$

where and  $\Gamma_5 = (0, 1) \times \{-1\}$ . The exact solution  $u$  yields

$$J_0(u) = \sqrt{0.5}, \quad J_1(u) = \sqrt{0.5}, \quad \text{and } J_2(u) = \log(1 + \sqrt{2}).$$



**Discretization** Here we use higher-order finite elements for discretization. We denote the configuration, where we used  $Q_r^c$  for the first primal problem and  $Q_{r+1}^c$  for the second primal problem and the dual problem, by  $Q_r/Q_{r+1}$  finite elements. We used

- $Q_1/Q_2$  finite elements.
- $Q_4/Q_5$  finite elements.
- $Q_8/Q_9$  finite elements.

*Remark 4.1.* In our numerical test we do not see any afford when using  $Q_r/Q_s$  finite elements, where  $s > r + 1$  in comparison to  $Q_r/Q_{r+1}$ . Since the latter is less computational work, we always use this FE combination.

**Discussion of our findings** In this example we do have a singularity in the right hand side and we are interested in the behavior of our algorithm if we use different finite element methods. For the  $I_{eff}$  we obtain the following results:

- $I_{eff} \in (0.5, 1.6)$  for  $Q_1/Q_2$  finite elements.
- $I_{eff} \in (0.07, 0.65)$  for  $Q_4/Q_5$  finite elements.
- $I_{eff} \in (0.15, 13.5)$  for  $Q_8/Q_9$  finite elements.

Observing our findings, we get an error estimator that works quite well if we use  $Q_1/Q_2$  finite elements, but it also seems that for a higher polynomial degree the error estimator gets worse. However if we take a look at Figure 21 we can see that the high and low values for higher polynomial degrees appear just at the beginning and the end of our algorithm. This may happen through the worse approximation due the coarse grid at the beginning and numerical errors at the end of our computation, because our error estimator just estimates the discretization error and not the numerical error. Nevertheless in the steps between, our error estimator is still better for  $Q_1/Q_2$  finite elements than for higher order.

As in the previous examples, we are also interested how the error is affected in the functionals of interest. For  $Q_1/Q_2$  finite elements we monitor in Figure 22 that we have a high inconsistency in the decrease of error and we even get some increases in both point evaluations. If we use higher polynomial degrees we nearly always have a similar reduction in all errors (except the end where the error for  $J_2$  increase because of numerical errors). Comparing the errors themselves we do get much better results if we use  $Q_4/Q_5$  finite elements or  $Q_8/Q_9$  finite elements. On the other hand, once we work with higher order we do not conclude an advantage of using very high polynomial degrees. Consequently, there is a big advantage of going from  $Q_1/Q_2$  to  $Q_4/Q_5$ . But even higher polynomial degrees do not pay off.

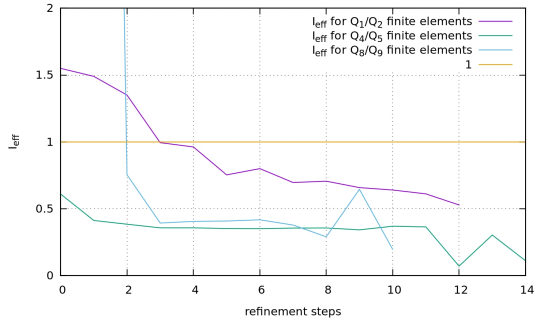


Figure 21:  $I_{eff}$  for example 3.

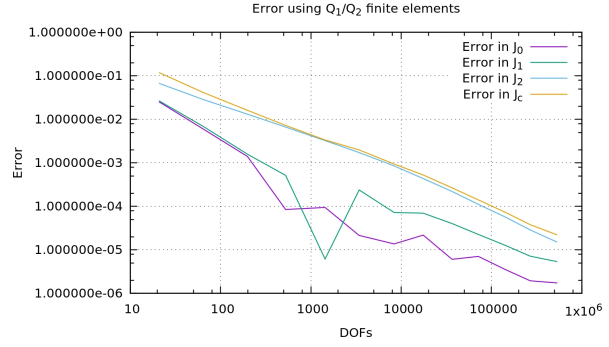


Figure 22: Example 3: Error using  $Q_1/Q_2$  finite elements.

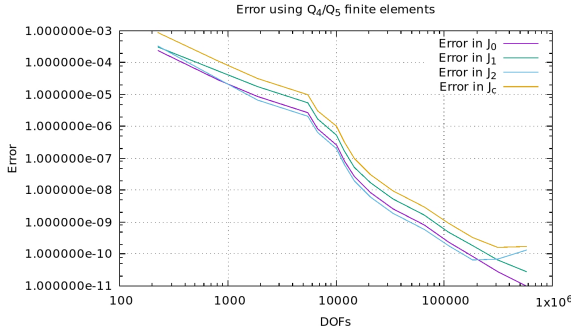


Figure 23: Example 3: Error using  $Q_4/Q_5$  finite elements.

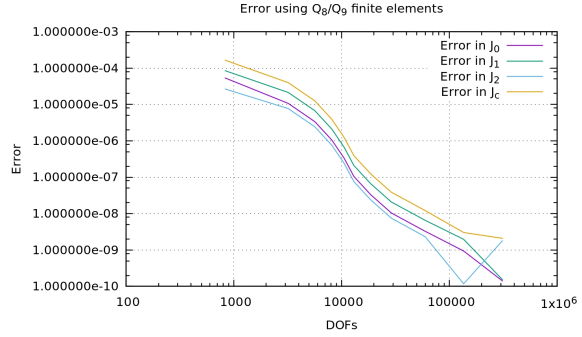


Figure 24: Example 3: Error using  $Q_8/Q_9$  finite elements.

We note that the error increase towards the maximal refinement steps in Figure 23 and Figure 24 results from numerical inaccuracies towards low tolerances, e.g., from solving the linear system or more likely that the flux evaluation, since we deal with a derivative, is not accurate enough. If we take a look at our refined meshes shown in Figure 26 - 28 we see that we always obtain refinements at the position of the singularity of the right hand side. This effect becomes stronger if we use polynomials with higher degree. Here, very localized mesh refinement is observed.

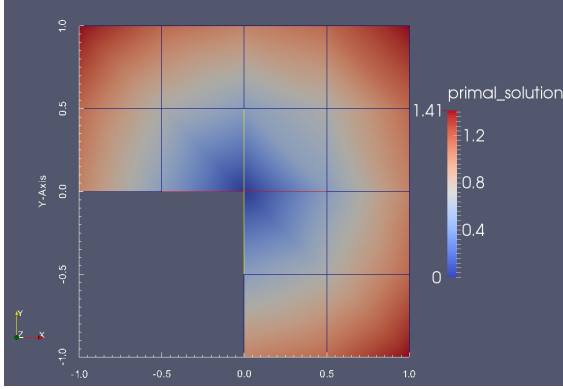


Figure 25: Initial mesh for example 3 (solution for  $Q_1/Q_2$  finite elements).

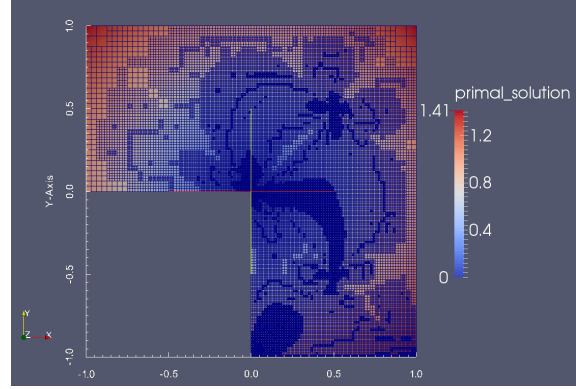


Figure 26: Example 3: Mesh for  $Q_1/Q_2$  finite elements after 9 refinement steps (71565 DOFs).

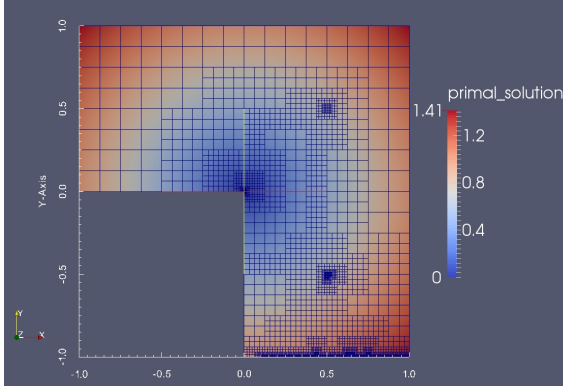


Figure 27: Example 3: Mesh for  $Q_4/Q_5$  finite elements after 10 refinement steps (65463 DOFs).

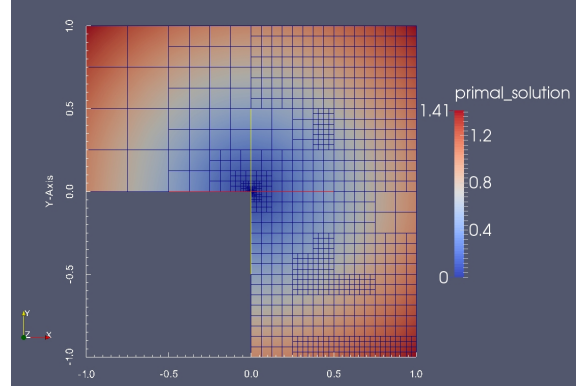


Figure 28: Example 3: Mesh for  $Q_8/Q_9$  finite elements after 8 refinement steps (59639 DOFs).

#### 4.4 Example 4a: a slit domain

In this final example we consider a slit domain with displacement discontinuity (which can be interpreted as a crack) as pictured in Figure 29. On the slit, homogeneous Neumann boundary conditions are prescribed. In Example 4a, nonhomogeneous Dirichlet and homogeneous Neumann conditions are prescribed on the outer boundary. In Example 4b, nonhomogeneous Dirichlet on the entire outer boundary are used for which, on the other hand, a manufactured solution can be constructed.

**Configuration** We consider the Laplace equation on a slit domain:

$$-\Delta u(x, y) = 0 \quad \forall (x, y) \in \Omega, \quad (42)$$

$$u(x, y) = g(x, y) \quad \forall (x, y) \in \Gamma_D, \quad (43)$$

$$\nabla u(x, y) \cdot n(x, y) = 0 \quad \forall (x, y) \in \Gamma_N, \quad (44)$$

where

$$\Omega = (-1, 1) \times (-1, 1) \setminus \{(x, 0) \mid -1 \leq x \leq 0\}. \quad (45)$$

The boundary parts are given as:

$$\Gamma_D = \{(-1, y) \mid -1 \leq y \leq 1\}, \quad (46)$$

$$\Gamma_N = \partial\Omega \setminus \Gamma_D, \quad (47)$$

and  $g(x, y)$  as

$$g(x, y) := \text{sign}(y) \frac{\lambda_{G_c}}{\sqrt{2}} \sqrt{\sqrt{x^2 + y^2} - x}, \quad (48)$$

and  $\lambda_{G_c} = 1$ . This coefficient is material parameter and related to the fracture toughness.

These conditions introduce a discontinuity on the boundary at  $(-1, 0)$  and consequently a crack with displacement discontinuity as displayed in Figure 29.

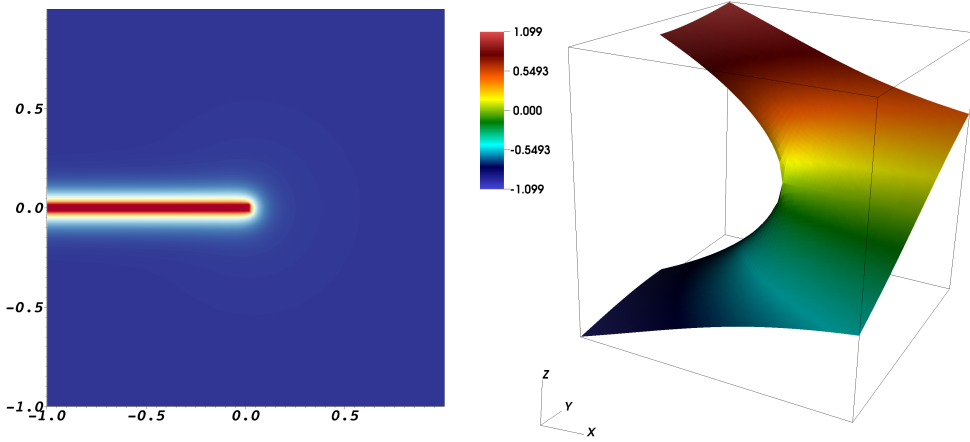


Figure 29: Example 4a: Discontinuity location (in red; left figure) and related numerical solution in a 3D plot (right) to Example 4b, which additionally highlights the non-homogeneous Dirichlet boundary conditions and the jump of displacements across the crack.

**Goal functionals of interest** We compute the following four goal functionals (but we notice that not always all goal functionals are simultaneously considered):

$$J_0(u) := u(0.75, 0.75), \quad J_1(u) := u(-0.5, -0.25), \quad (49)$$

$$J_2(u) := \int_{\Gamma_6} \nabla u(x, y) \cdot n \, d(x, y), \quad J_3(u) := \int_{\Omega_6} u(x, y) \, d(x, y), \quad (50)$$

where  $\Gamma_6 = \{-1\} \times (-1, -0.25)$  and  $\Omega_6 = (0, 1) \times (-1, 0)$ .

However no exact solution is known therefore we approximate the exact functionals by values that obtained from a very fine mesh:

- $J_0(u) \approx 0.18949212064$
- $J_1(u) \approx -0.66061009755$
- $J_2(u) \approx -0.54411579542$
- $J_3(u) \approx -0.18268521784$

**Discretization** As in Example 1a.

**Discussion of our findings** First, we consider detailed studies for a single goal functional. The reason is that this test might serve as kind of benchmark for testing algorithms which compute fractures. Even for single goal functionals the existing literature is rare. A fracture is nothing else than a discontinuity along a line in the primal solution. Thus the slit domain is a limiting case for a fracture setting. After having revisited a single goal functional, we add as in the previous examples more quantities of interest. We use 4 different configurations for our goal functionals:

- Config. 1 : Evaluating  $J_0(u)$ .
- Config. 2 : Evaluating  $J_0(u)$  and  $J_1(u)$ .
- Config. 3 : Evaluating  $J_0(u)$ ,  $J_1(u)$  and  $J_2(u)$ .
- Config. 4 : Evaluating  $J_0(u)$ ,  $J_1(u)$ ,  $J_2(u)$  and  $J_3(u)$ .

In Figure 30 we see that in all configurations we underestimate the error in  $J_c$ , but we cannot expect to have  $I_{eff} = 1$  for this problem due to the loss of regularity. Furthermore the  $I_{eff}$  seems not to differ that much for the different configurations. In the Figures 31 - 34 we can observe that for all configurations we get a much better reduction for our refinement if we compare it to global refinement. An interesting aspect is that in this example all errors are of similar order and we also have a similar reduction in the error.

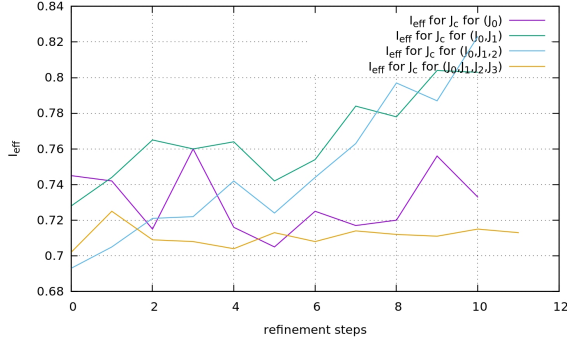


Figure 30: Example 4a:  $I_{eff}$  for Configuration 1-4.

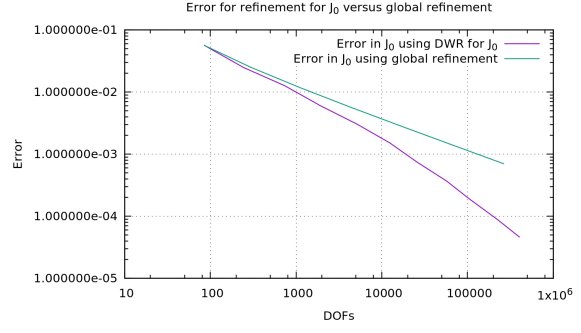


Figure 31: Example 4a: Error for Configuration 1.

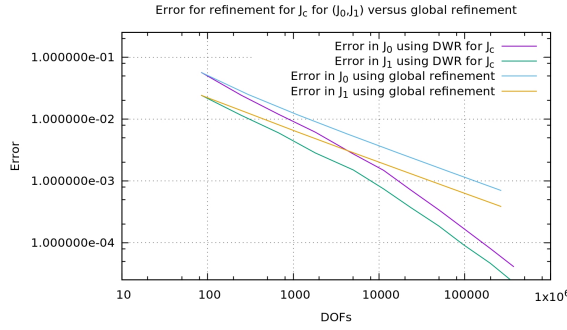


Figure 32: Example 4a: Error for Config. 2.

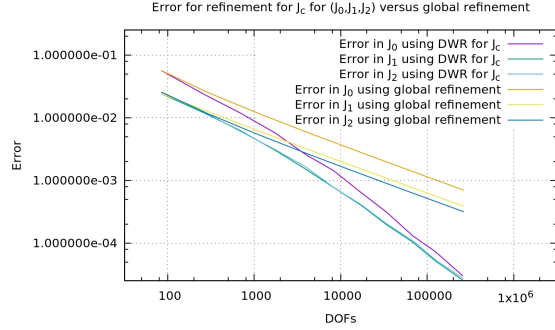


Figure 33: Example 4a: Error for Config. 3.

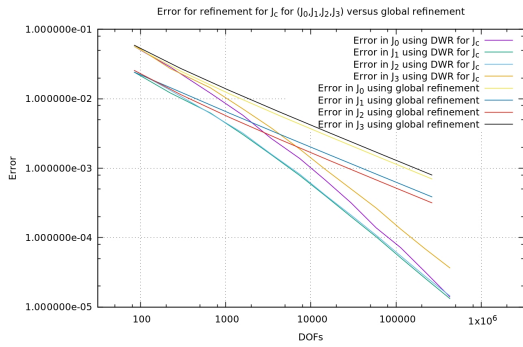


Figure 34: Example 4a: Error for Config. 4.

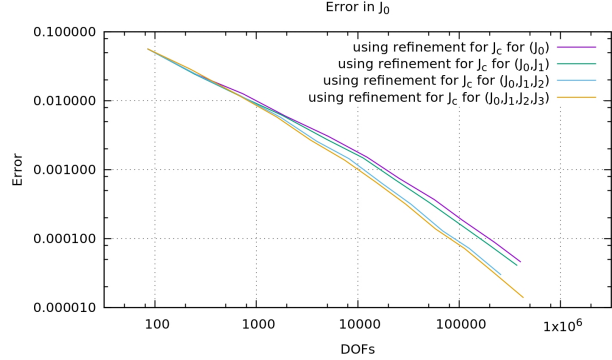


Figure 35: Example 4a: Error for  $J_0$  for Configuration 1-4.

Another interesting observation can be made in Figure 35 where we even obtain better results if we refine for  $J_c$  instead for  $J_0$ . Usually we would expect a worse result if we try to refine for more than one functional at the same time. But unfortunately we do not have that in general as it can be monitored in Figure 5 for  $J_2$ . Nevertheless we observe that the results are also good for less regular problems even if the error estimator is not that

accurate. But we find that our refinement scheme also takes care of low regularity domains for all our configurations as displayed in Figure 36-39 for which the initial mesh is shown in Figure 49.

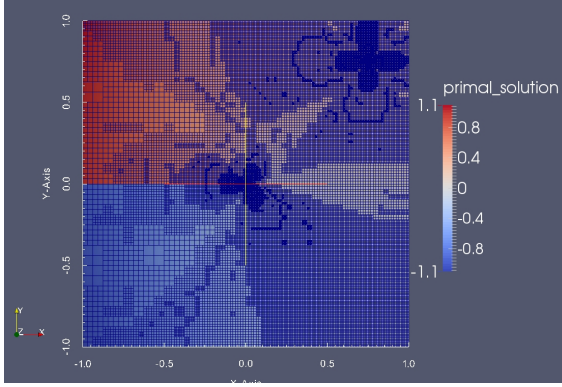


Figure 36: Example 4a: Mesh for Config. 1 after 7 refinement steps (56809 DOFs).

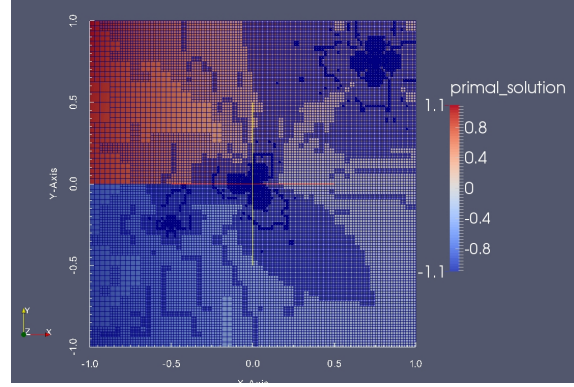


Figure 37: Example 4a: Mesh for Config. 2 after 7 refinement steps (49883 DOFs).

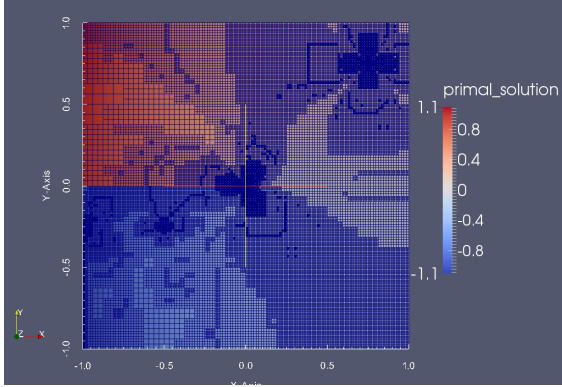


Figure 38: Example 4a: Mesh for Config. 3 after 8 refinement steps (68809 DOFs).

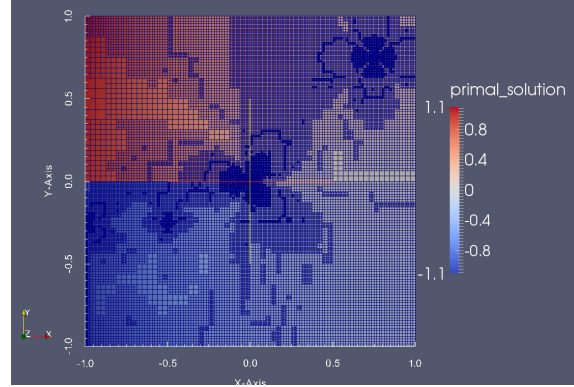


Figure 39: Example 4a: Mesh for Config. 4 after 8 refinement steps (58425 DOFs).

#### 4.4.1 Example 4b: a slit domain

As in Example 4a we consider the Laplace equation on a slit domain with displacement discontinuity (i.e., the crack) as pictured in Figure 29. The domain and location of the crack are chosen in such a way that we can work with the manufactured solution constructed in [10, 3]:

$$u(x, y) = \lambda_{G_c} r^{1/2} \sin(\varphi/2),$$

where  $\lambda_{G_c} = 1$  in polar coordinates and Cartesian coordinates:

$$u(x, y) = \text{sign}(y) \frac{\lambda_{G_c}}{\sqrt{2}} \sqrt{\sqrt{x^2 + y^2} - x}.$$

Now we prescribe

$$g(x, y) := \text{sign}(y) \frac{\lambda_{G_c}}{\sqrt{2}} \sqrt{\sqrt{x^2 + y^2} - x}, \quad (51)$$

on the entire outer boundary.

**Goal functionals of interest** We consider the following four goal functionals (here we are not always interested in all goal functionals):

$$J_0(u) := u(0.75, 0.75), \quad J_1(u) := u(-0.5, -0.25), \quad (52)$$

$$J_2(u) := \int_{\Gamma_7} \nabla u(x, y) \cdot n \, d(x, y), \quad J_3(u) := \int_{\Omega_7} u(x, y) \, d(x, y), \quad (53)$$

where and  $\Gamma_7 = \{-1\} \times (-1, -0.25)$  and  $\Omega_6 = (0, 1) \times (-1, 0)$ .

**Discretization** Here we use different FE for discretization (as in Example 3). We denote the configuration, where we used  $Q_r^c$  for the first primal problem and  $Q_{r+1}^c$  for the second primal problem and the dual problem, by  $Q_r/Q_{r+1}$  finite elements. We used

- $Q_1/Q_2$  finite elements.
- $Q_2/Q_3$  finite elements.
- $Q_3/Q_4$  finite elements.
- $Q_4/Q_5$  finite elements.

**Discussion of our findings** In this example, we also perform studies for different polynomial degrees. Furthermore we are interested in how the error decreases with respect to the number of refinement steps. Here we observe that for all tested polynomial degrees we achieve a similar decrease as  $O(h)$  for global refinement, i.e. the error of every functional for both refinement methods and all tested polynomial degrees is approximately halved in very refinement step as we detect in Figure 40-43. Therefore we almost get the same behavior as global refinement in the errors if we just compare it to the refinement steps. However as we monitor in Figure 44 we save many DOFs for our refinement scheme in comparison to global refinement (behaves like  $O(h^{-2})$ ) for almost the same accuracy. If we now compare the different polynomial degrees we observe that for a higher polynomial degree we start with a higher number of DOFs but we do get a less increase than for lower polynomial degree such that we get less DOFs for a higher polynomial degree after a certain number of refinement steps. With regard to the maximal number of DOFs, we remark that the plot curves for global refinement stop because we did not solve linear systems with more than 1 100 000 unknowns. The behavior of the latter refinement steps shown in Figure 42 and Figure 43 results from numerical errors.



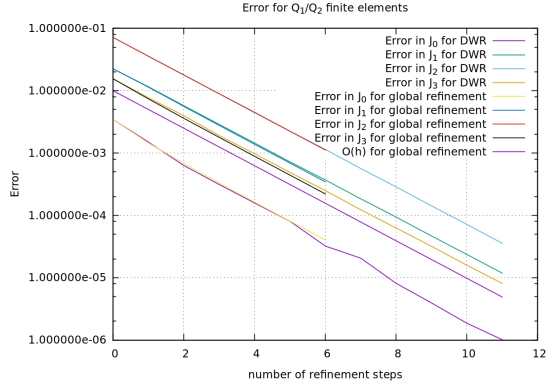


Figure 40: Example 4b: Error versus refinement steps for  $Q_1/Q_2$  finite elements.

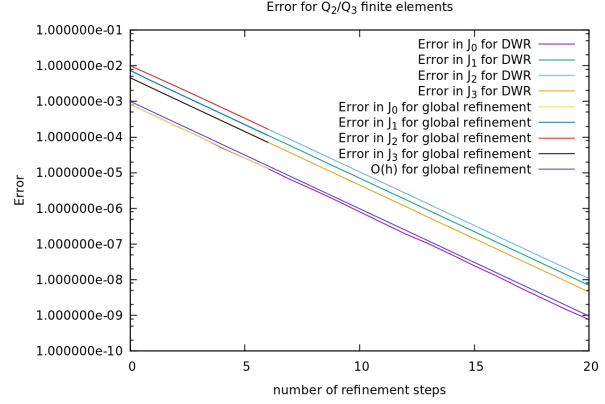


Figure 41: Example 4b: Error versus refinement steps for  $Q_2/Q_3$  finite elements.

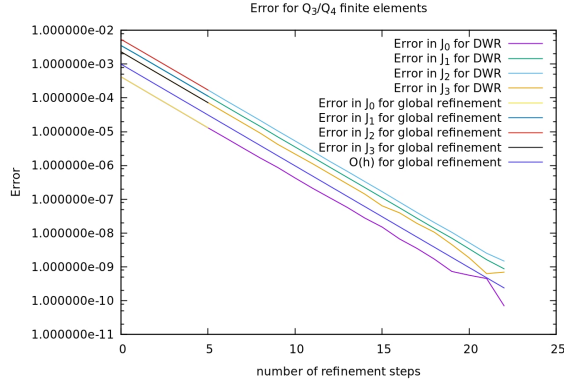


Figure 42: Example 4b: Error versus refinement steps for  $Q_3/Q_4$  finite elements.

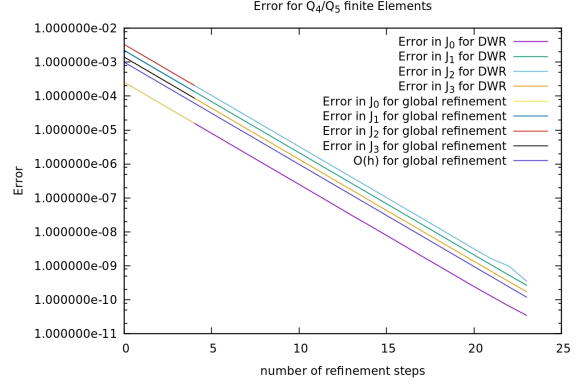


Figure 43: Example 4b: Error versus refinement steps for  $Q_4/Q_5$  finite elements.

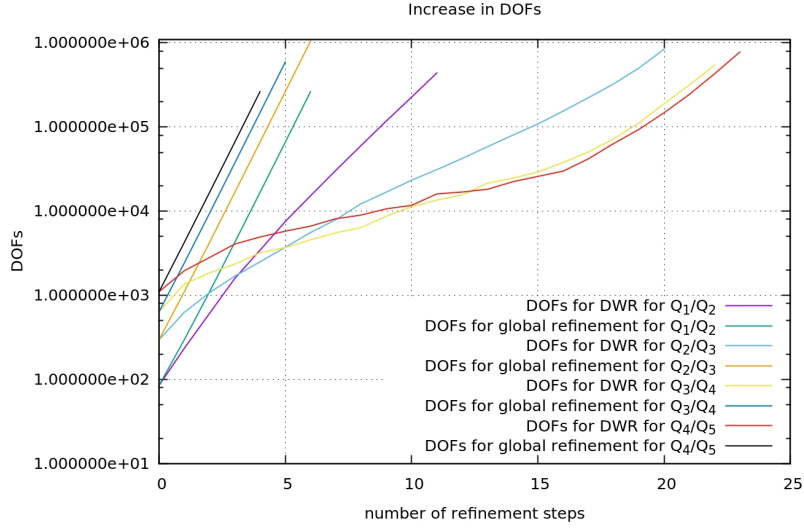


Figure 44: Example 4b: Increase in DOFs for different finite elements and refinement schemes.

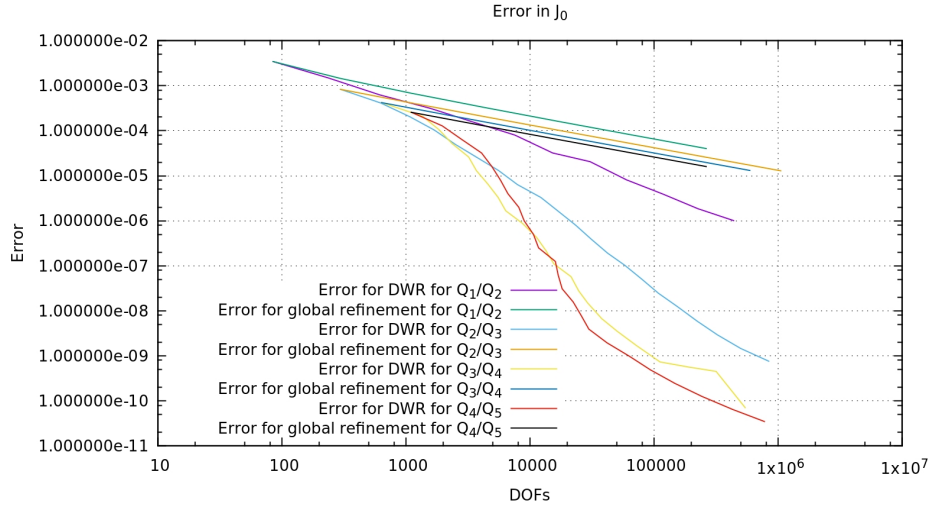


Figure 45: Example 4b: Error in  $J_0$  for different finite elements and refinement schemes.

But as we visualize in Figure 44 the advantage of  $Q_4/Q_5$  finite elements compared to  $Q_3/Q_4$  finite elements is not as big as if we compare  $Q_3/Q_4$  and  $Q_2/Q_3$  finite elements. Since all errors for all polynomial degrees show a similar behavior we just take a look at the error in  $J_0$  in this example. If we plot the error in  $J_0$  against the DOFs as shown in Figure 45 we can see the advantage of Algorithm 3.1. Here we can again see the advantage of using higher polynomial degrees. To reach an error less than  $10^{-6}$  we need for  $Q_1/Q_2$  finite elements of about  $5 \times 10^5$  DOFs and for  $Q_4/Q_5$  finite elements of about 9000 DOFs. But also the findings for  $Q_1/Q_2$  finite elements are satisfying in comparison to global refinement for all tested polynomial degrees. By taking a look at the meshes constructed by our algorithm

(Figure 46-48), one can observe that for higher polynomial degrees more refinements in low regularity regions than in specific functional areas take place. This is in agreement with our findings in Example 3.

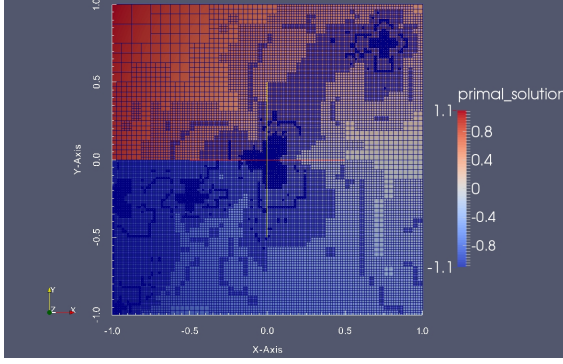


Figure 46: Example 4b: Mesh and solution for  $Q_1/Q_2$  finite elements after 8 refinement steps (60119 DOFs).

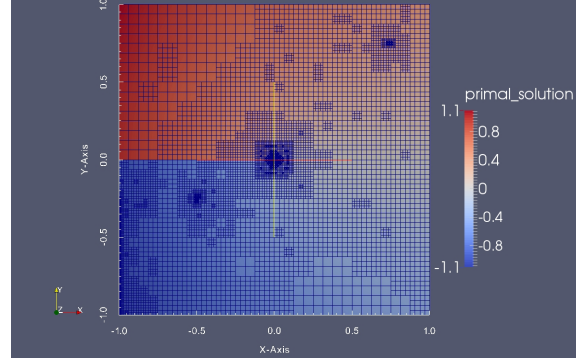


Figure 47: Example 4b: Mesh and solution for  $Q_2/Q_3$  finite elements after 18 refinement steps (58289 DOFs).

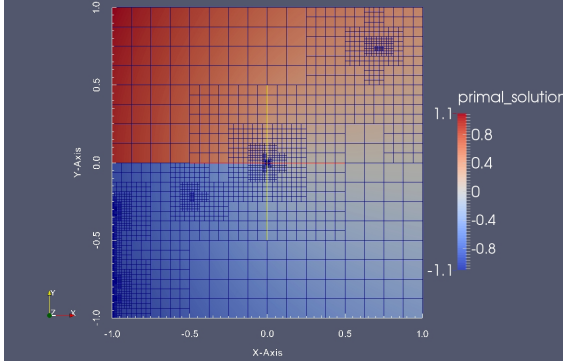


Figure 48: Example 4b: Mesh and solution for  $Q_4/Q_5$  finite elements after 18 refinement steps (63403 DOFs).

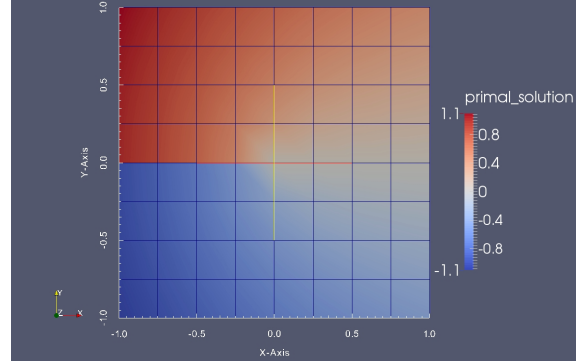


Figure 49: Example 4b: Initial mesh for Example 4a ( $Q_4/Q_5$  solution for example 7).

## 5 Conclusions

In this work, we further developed dual-weighted residual error estimation for multiple goal functionals applied to elliptic problems. First, we addressed a weak localization of the error estimator using a partition-of-unity. Next, we proposed an alternative way to solve the dual-dual problem. In the last section, we provided extensive numerical computations for various domains, different types of goal functionals, and different boundary conditions as well as higher-order finite element calculations. From our observations we can deduce that the functional  $J_c$  (introduced in (23)) delivers a similar behavior than the functional, contained in  $\mathbb{J}$ , with the highest relative error if the self-chosen weights  $\omega_i$  from (23) are equal. This leads to a better decrease in the error of this functional but not necessarily for the other functionals (as shown in Example 2a). However we do obtain a better decrease in the maximal relative error than global refinement, which was subject of our investigation in Section 3. If the errors in the different functionals are of similar order than we observe that we achieve a decrease in every functional as the Figures 23 and 24 and Figures 32-34 show. Example 2b demonstrates that the computation of the sign of the procedure described in Section 3.1 can unfortunately not be avoided. We found out that there can be a big advantage using a higher polynomial degree, even we may get a worse error estimator (as shown in Example 3). Furthermore we also obtained very good findings for a problem on a low regularity domain (as shown in Example 4a). Also for singular right hand sides we obtain satisfying results and we found that for higher polynomial degrees we do more refinement steps at the low regularity regions (as shown in Example 3). We briefly comment that we also observed the general benefit of using an adaptive algorithm: using global refinement limits significantly to reach low tolerances because the linear systems are simply too big and memory-consuming. For instance, in Example 4b we could only reach a tolerance of  $10^{-5}$  using global mesh refinement. Finally, we notice that the last test, namely Example 4, might serve as basis for developing mesh adaptivity for sophisticated computational methods for treating fracture (or damage) settings (in which the crack is not nicely aligned with the mesh) such as extended/generalized finite elements or phase-field methods. Thus the provided methodology has an immediate potential to be extended for current practical applications.

## Acknowledgments

We want to thank Professor Ulrich Langer for supporting this work at the Institute of Computational Mathematics at JKU Linz.

## References

- [1] M. Ainsworth and J. T. Oden. A posteriori error estimation in finite element analysis. *Computer Methods in Applied Mechanics and Engineering*, 142(1-2):1–88, 1997.
- [2] M. Ainsworth and J. T. Oden. *A Posteriori Error Estimation in Finite Element Analysis*. Pure and Applied Mathematics (New York). Wiley-Interscience [John Wiley & Sons], New York, 2000.

- [3] J. Andersson and H. Mikayelyan. The asymptotics of the curvature of the free discontinuity set near the cracktip for the minimizers of the Mumford-Shah functional in the plain. a revision. arXiv: 1205.5328v2, 2015.
- [4] T. Apel, A.-M. Saendig, and J. R. Whiteman. Graded mesh refinement and error estimates for finite element solutions of elliptic boundary value problems in non-smooth domains. *Mathematical Methods in the Applied Sciences*, 19(1):63–85, 1996.
- [5] W. Bangerth, R. Hartmann, and G. Kanschat. deal.II – a general purpose object oriented finite element library. *ACM Trans. Math. Softw.*, 33(4):24/1–24/27, 2007.
- [6] W. Bangerth, T. Heister, and G. Kanschat. *Differential Equations Analysis Library*, 2012.
- [7] W. Bangerth and R. Rannacher. *Adaptive Finite Element Methods for Differential Equations*. Birkhäuser, Lectures in Mathematics, ETH Zürich, 2003.
- [8] R. Becker and R. Rannacher. Weighted a posteriori error control in FE methods. In e. a. H. G. Bock, editor, *ENUMATH’97*. World Sci. Publ., Singapore, 1995.
- [9] R. Becker and R. Rannacher. *An optimal control approach to error control and mesh adaptation in finite element methods*, pages 1–102. Acta Numerica 2001, Cambridge University Press, a. iserles edition, 2001.
- [10] A. Bonnet and G. David. *Cracktip is a global Mumford-Shah minimizer*. Asterisque No. 274, 2001.
- [11] M. Braack and A. Ern. A posteriori control of modeling errors and discretization errors. *Multiscale Model. Simul.*, 1(2):221–238, 2003.
- [12] G. F. Carey and J. T. Oden. *Finite Elements. Volume III. Computational Aspects*. The Texas Finite Element Series, Prentice-Hall, Inc., Englewood Cliffs, 1984.
- [13] C. Carstensen and R. Verfürth. Edge residuals dominate a posteriori error estimates for low order finite element methods. *SIAM J. Numer. Anal.*, 36(5):1571–1587, 1999.
- [14] D. Estep, M. Holst, and M. Larson. Generalized green’s functions and the effective domain of influence. *SIAM Journal on Scientific Computing*, 26(4):1314–1339, 2005.
- [15] L. C. Evans. *Partial differential equations*. American Mathematical Society, 2010.
- [16] M. Giles and E. Süli. Adjoint methods for pdes: a posteriori error analysis and post-processing by duality. *Acta Numerica 2002*, pages 145–236, 2002. A. Iserles, ed.
- [17] C. Großmann, H.-G. Roos, and M. Stynes. *Numerical Treatment of Partial Differential Equations*. Springer, 2007.
- [18] R. Hartmann. Multitarget error estimation and adaptivity in aerodynamic flow simulations. *SIAM Journal on Scientific Computing*, 31(1):708–731, 2008.

- [19] R. Hartmann and P. Houston. Goal-oriented a posteriori error estimation for multiple target functionals. In T. Hou and E. Tadmor, editors, *Hyperbolic Problems: Theory, Numerics, Applications*, pages 579–588. Springer Berlin Heidelberg, 2003.
- [20] P. Houston, B. Senior, and E. Sueli. hp-discontinuous galerkin finite element methods for hyperbolic problems: error analysis and adaptivity. *International Journal for Numerical Methods in Fluids*, 40(1-2):153–169, 2002.
- [21] D. Kuzmin and S. Korotov. Goal-oriented a posteriori error estimates for transport problems. *Math. Comp. Sim.*, 80(8):1674 – 1683, 2010.
- [22] J. Oden and S. Prudhomme. On goal-oriented error estimation for elliptic problems: Application to the control of pointwise errors. *Comput. Methods Appl. Mech. Engrg.*, 176:313–331, 1999.
- [23] J. Peraire and A. Patera. Bounds for linear-functional outputs of coercive partial differential equations: local indicators and adaptive refinement. In P. Ladeveze and J. Oden, editors, *Advances in Adaptive Computational Methods in Mechanics*, pages 199–215. Elsevier, Amsterdam, 1998.
- [24] R. Rannacher and F.-T. Suttmeier. A feed-back approach to error control in finite element methods: application to linear elasticity. *Computational Mechanics*, 19(5):434–446, 1997.
- [25] T. Richter. Goal-oriented error estimation for fluid-structure interaction problems. *Comp. Methods Appl. Mech. Engrg.*, 223-224:38–42, 2012.
- [26] T. Richter and T. Wick. Variational localizations of the dual weighted residual estimator. *Journal of Computational and Applied Mathematics*, 279(0):192 – 208, 2015.
- [27] A. Schroeder and A. Rademacher. Goal-oriented error control in adaptive mixed {FEM} for signorinis problem. *Computer Methods in Applied Mechanics and Engineering*, 200(14):345 – 355, 2011.
- [28] E. van Brummelen, S. Zhuk, and G. van Zwieten. Worst-case multi-objective error estimation and adaptivity. arXiv:1604.04541v1, 2016.
- [29] R. Verfürth. *A Review of A Posteriori Error Estimation and Adaptive Mesh-Refinement Techniques*. Wiley/Teubner, New York-Stuttgart, 1996.
- [30] T. Wick. Goal functional evaluations for phase-field fracture using pu-based dwr mesh adaptivity. *Computational Mechanics*, pages 1–19, 2016.
- [31] K. Zee, E. Brummelen, I. Akkerman, and R. Borst. Goal-oriented error estimation and adaptivity for fluid-structure interaction using exact linearized adjoints. *CMAME*, 200:2738–2757, 2011.